

**Recent Advancements in Rational Design of Non-Aqueous Organic Redox Flow Batteries**

Journal:	<i>Sustainable Energy &amp; Fuels</i>
Manuscript ID	SE-REV-05-2020-000800.R1
Article Type:	Review Article
Date Submitted by the Author:	11-Jul-2020
Complete List of Authors:	Li, Min; University of Utah, Department of Chemistry Rhodes, Zayn; University of Utah, Department of Chemistry Cabrera-Pardo, Jaime; University of Utah, Department of Chemistry Minteer, Shelley; University of Utah, Department of Chemistry

## ARTICLE

## Recent Advancements in Rational Design of Non-Aqueous Organic Redox Flow Batteries

Received 00th May 2020,  
Accepted 00th January 20xx

Min Li<sup>a,b,\*</sup>, Zayn Rhodes<sup>a,b</sup>, Jaime R. Cabrera-Pardo<sup>a,b</sup>, Shelley D. Minteer<sup>a,b,\*</sup>

DOI: 10.1039/x0xx00000x

In this review, we summarize the state-of-the-art advancements made in organic redox flow batteries (ORFBs) with special emphasis on non-aqueous (NAq) electrolytes. ORFBs utilize earth-abundant and potentially cost-effective organic redox-active molecules (ORMs), and have rapidly gained scientific interest. Transitioning from aqueous (Aq) solvents to NAq electrolytes expands the stable electrochemical windows available in ORFBs, thus offering great potential to increase both power density and energy density. To combine the advantages of ORM and NAq electrolytes, non-aqueous organic redox flow batteries (NAqORFBs) have emerged. Recent advances in NAqORFBs have focused on the development of ORM with large redox potential differences, multi-electron transfer capabilities, improved solubility, and stability. Strategies for preventing the crossover of redox-active species have also been documented. Collectively, these studies potentiate NAqORFBs as an important approach for sustainable energy storage. Still greater opportunities to further increase the battery performance through increased energy density, energy efficiency, and cycling lifetime can be realized by molecular engineering of ORM and rational design of battery cells. We, therefore, review the critical principles that require to be considered in engineering NAqORFBs, and conclude a discussion of emerging possibilities in these areas.

### Introduction

Redox flow batteries (RFBs) that circulate fluid electroactive materials between liquid electrolyte tanks and electrochemical cells have shown great promise in grid-scale energy storage.<sup>1-4</sup> Unlike enclosed batteries (e.g., lithium-ion batteries and lead-acid batteries) in which energy is stored in the electrode materials, RFBs enable energy storage in the liquid electrolyte contained in external tanks, and power generation as the electrolyte flows through an electrochemical cell reactor where electrons are harvested and channeled through an external circuit. The integration of circulating electroactive liquids with their reversible redox electrochemistry allows RFBs to function as both fuel cells and batteries. Accordingly, RFBs decouple power rating (reactor size) and energy capacity (tank size), offering distinct advantages in battery scalability, high power input, and output. The first RFB-like cell was documented in 1980s,<sup>5</sup> while until recently, prompted by the renaissance of renewable electricity generators, extensive studies in the redox chemistry and technical essentials in improving the performance of RFBs have been currently ongoing worldwide.<sup>6-8</sup> The unique technical perspective of RFBs in decoupling power and energy indicates the great potential in applications including the integration of renewable

power and conversion of electrical energy into chemical energy in the range of KW/KW h to MW/WM h.<sup>9</sup>

Despite the tremendous progress made in RFBs, they remain in the early stages of development. For instance, challenges associated with the choice of redox-active species are under intense scrutiny.<sup>10-12</sup> Currently, employment of metal-based inorganic molecules as electroactive species is dominant in the market, of which all-vanadium redox-flow batteries (VRFBs)<sup>13</sup> are the most developed flow battery systems, and are commercially available around the globe.<sup>14</sup> The facile electrochemical reversibility, and the wide span between the standard reduction potential of  $V^{2+}/V^{3+}$  and  $VO^{2+}/VO_2^+$  couples grant VRFBs high energy efficiency and relatively large power output. More importantly, V is the only redox-active metal element for both catholyte and anolyte. This 'symmetric' architecture allows for electrolyte regeneration when ions cross the membrane and provides the ability to restore capacity by simply mixing electrolytes periodically.<sup>15</sup> However, current VRFBs, face several crucial challenges for deep market penetration.<sup>13</sup> First, the availability of V species along with a maximum active material solubility restrict the further improvement of energy density ( $<25 \text{ Wh L}^{-1}$  in many flow battery systems).<sup>5</sup> To prevent thermal precipitation of vanadium ions in sulfuric acid, active temperature regulation systems are often incorporated to maintain VRFB operational between 10 and 40 °C.<sup>13</sup> Most critically, expensive vanadium resources and ion-exchange membranes inflate the capital cost of VRFB systems up to 800/kWh,<sup>16,17</sup> while the cost target set by the U.S. Department of Energy (DOE) is \$100/kWh. Other issues, including highly

<sup>a</sup> Department of Chemistry, University of Utah, 315 South 1400 East, Salt Lake City, UT, 84112, United States.

<sup>b</sup> Joint Center for Energy Storage Research (JCESR), United States.

\* Corresponding authors, Min Li, min.li@chem.utah.edu;  
Shelley D. Minteer, minteer@chem.utah.edu.

corrosive cell environment, and gas evolution have also plagued VRFBs.<sup>13</sup> Consequently, it is imperative to investigate alternative electroactive materials that are 'green' and cost-effective for the wide-scale utilization of RFBs.

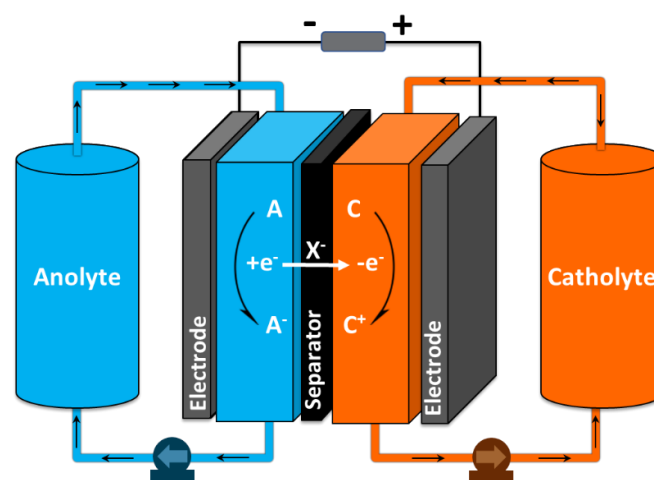
Organic molecules have recently received considerable attention in the RFB community as possible replacements for metal-based materials.<sup>18</sup> Different from transition metal salts, organic redox-active species (ORMs) are typically composed of earth-abundant elements, and can be synthesized *via* sustainable and low-cost materials. Although organic redox flow batteries (ORFBs) are still in the early stages of development, \$27/kW h of chemical cost has been demonstrated – a third of the cost of vanadium electrolytes (\$81/kW h).<sup>19</sup> Additionally, while the number of inorganic redox couples is limited, the possibility of organic redox species can be numerous. Molecular engineering of ORM to implement necessary properties creates new possibilities in a diversity of domains in RFBs.<sup>20–22</sup> Examples include tailored molecules with tunable reduction potential,<sup>19</sup> improved solubility,<sup>23</sup> and multiple electron transfer capability.<sup>24</sup> In line with molecular engineering, there has been a surge of interest in evaluating new organic molecules to expand cell voltage.<sup>25–27</sup> The resultant large cell voltage ( $\geq 2.0$  V) offer great opportunities to improve energy density. Meanwhile, due to the narrow electrochemical window of aqueous electrolytes ( $< 1.5$  V), nonaqueous solutions are required for operation. Thus, the use of these nonaqueous electrolytes greatly expands the design space for exploring a variety of cathode and anode-active organics. Through the combination of these solvents and large voltage gap ORM, NAQORFBs are believed to be critical in developing low-cost, sustainable, and versatile RFBs.

In the current review, we summarize the current state of RFBs with special emphasis on non-aqueous electrolytes. Reviews about RFBs employing aqueous systems have been discussed elsewhere in literature.<sup>28–30</sup> It is worth noting again that the use of nonaqueous electrolytes is of great significance in developing next-generation RFBs because it opens up many possibilities, including evaluation of abundant redox active species, molecular engineering for functionalization, and investigation of various nonaqueous solvent alternatives to improve battery performance. Advances in any of these are crucial to enhance the energy density and power density of RFBs. Owing to the burgeoning investigation and rapid progress in NAQORFBs, reviews have been published to cover electroactive organic molecules<sup>1,2,31,32</sup> (e.g., radicals,<sup>33</sup> polymers,<sup>34</sup> and carbonyl compounds<sup>10,22</sup>) synthesized to improve battery performance. Here we do not seek to reiterate these extensive compilations of the state-of-the-art, but rather give insight into the engineering strategies developed in order to improve the power density and energy density of NAQORFBs. While molecular engineering of ORM has been documented, what distinguishes the current work from the existing literature is that we screen the state-of-the-art advancements made in NAQORFBs, shed light upon the approaches that lie behind the developments, and detail the areas of particular interest through highlighted examples. Further, system optimization aided by computational modeling

has been incorporated. This analysis bridges the scientific aspects of NAQORFBs with ongoing practices, and is anticipated to facilitate the improvement of versatile ORM. Topics to be covered include strategies for enabling multielectron transfer, improving solubility, cell voltage, and species crossover. Finally, we will address current limitations and challenges to the extended application of NAQORFBs. Future directions toward the rational design of redox-active materials are also suggested.

## I. Engineering Principles of Redox Flow Batteries

Recent advances in ORFBs have demonstrated substantial potential in the choice of organic materials, electrodes and membranes to develop next-generation batteries. While strategies used for functionalization may vary, the principles of molecular engineering are shared in most RFBs. Because RFBs are different from conventional solid-state batteries, the working principles and performance metrics as a response to the battery architectures are also different. Therefore, we first describe the general structure of RFBs and their components and examine the roles of each in battery operation.



**Scheme 1.** Illustration of the structure and charging process of redox flow batteries. During battery charging, ions from supporting electrolytes cross through the separator for charge balance, while active species are blocked to prevent battery from self-discharge.

As illustrated in [Scheme 1](#), a typical RFB consists of two liquid storage tanks and an electrochemical reactor with embedded membrane and electrodes. Redox-active compounds are dissolved in supporting electrolytes, and pumped through the cell where electrochemical reactions occur. The membrane employed in the cell reactor separates catholyte and anolyte redox active species, while allowing charge carriers from the supporting electrolytes to cross through for charge balance. Upon charging, electricity drives redox reactions at the electrodes and energy is stored chemically in the electrolytes, while in the discharging process,

chemical energy is converted back into electrical energy. The key structure is the circulation system that enables pumping of the liquid electrolytes between the storage tanks and the electrochemical cell. Accordingly, RFBs allow storage of grid-scale energy in the redox-active liquids, and subsequently generate power continuously through pumping the charged liquid electrolytes to the electrodes. Because the liquid tanks and the electrochemical cell are separate, it is possible to independently optimize the energy storage capacity and power output for a variety of applications.

Mathematically, the theoretical energy density ( $E_d$ ) and power density ( $P_d$ ) provided by a RFB can be calculated by the following equations:

$$E_d = \frac{nCFV}{\mu_v} \quad (1)$$

$$P_d = \frac{I \times V}{S} \quad (2)$$

Where  $n$  is the number of electrons transferred in the redox electrochemistry,  $C$  is the lower concentration of the two active electrolytes,  $F$  is the Faraday's constant,  $V$  is the battery voltage,  $I$  is the discharging current,  $S$  is the active surface area of a RFB, which is normally referred to the effective area of the electrode.  $\mu_v$  is the volume factor, which is defined as 1 plus the ratio of lower electrolyte concentration over higher electrolyte concentration.

Consequently, the energy density of a RFB system is determined by the concentration, the number of electrons

electrolytes (e.g., redox potential, solubility, stability, reaction kinetics) have many impacts on both the energy density and power density of a redox flow battery. As a result, molecular engineering of organic materials, including redox-active species and supporting electrolytes provides a simple, robust, and versatile approach for enhancing the performance of RFBs.

Another critical factor that may cause detrimental effects on the discharge current is the crossover of redox-active species. Ideally, the embedded membrane (Scheme 1) only allows supporting electrolytes to pass through with rapid transport to obtain high coulombic efficiency. However, many RFB systems suffer from this chemical crossover, leading to capacity decay during cycling. Another problem encountered in this regard is ORMs degradation. Not surprisingly, these findings have elicited substantial interest in exploring organic alternatives and characterization techniques to resolve the issues. Examples include the development of active polymeric materials, incorporation of conjugated structures, and evaluation of size-exclusion membranes. Nevertheless, the prevention of species crossover and decomposition continues to be an important challenge.

Taking these analyses as inspiration, we review the strategies developed for addressing challenges in advancing energy density and power density of NAqORFB. These strategies include designing molecules with low melting points, accessing second electron transfers, extending the redox potential gap to increase the output voltage, minimizing

**Table 1.** Summary of seminal ORMs that have been investigated for improving solubility in non-aqueous solvents.

ORMs	mp. (°C)	Solubility		Ref.
		Pure Solvent	Solvent/Salt	
TEMPO	36 - 38	5.2 M in EC/PC/EMC	2.0 M in 2.3 M LiPF <sub>6</sub> /EC/PC/EMC	35
BzNSN	42 - 44	5.7 M in MeCN	2.1 M in 2.1 M LiTFSI/MeCN	36
Quinoxaline	29 - 32	7.0 M in PC	-	37
DBBB	69.3 - 70.1	Ca. 0.4 M in PC	Ca. 0.3 M in 0.5 M LiTFSI/PC	38, 39
ANL-8	< 25	miscible	miscible	40
23DDB	> 25	-	2.0 M in 0.5 M LiTFSI/PC	39
EPT	103 - 104	0.25 M in MeCN	0.1 M in 0.5 TEABF <sub>4</sub> /MeCN	41
MEEPT	< 25	miscible	miscible	41
NMe-DAAQ	265 - 269	0.02 M in MeCN	0.016 M in 1.0 M LiTFSI/MeCN	42
Me-TEG-DAAQ	25	1.04 M in MeCN	1.02 M in 1.0 M LiTFSI/MeCN	42
NMePh	132 - 136	< 0.7 M in DME	-	43
LiTFSI/NMePh/urea	< 25	4.0 M in DES	-	44
DMFc/BuPh	< 25	3.5 M in DES	-	45

transferred per redox-active molecule, and the redox potential of redox-active species pair. As for the power density, while the battery voltage and effective surface area of the electrodes are often easily determined, the discharge current is dependent on many factors, including the reaction kinetics of electrolytes, the solution conductivity, electrodes, and operation conditions (e.g. temperature and flow rate). Although stacking multiple cells provides higher power density, increased cost, and manufacturing complexity are a potential consequence. In contrast, the properties possessed by

crossover and enhancing electrochemical stability. We examine how each approach has been explored and used to enhance battery performance and their relative strengths and weaknesses. Last, we discuss future opportunities and needs that may help to realize a deeper understanding of NAqORFB, and eventually widespread implementation.

## II. Strategies in Advancing NAqORFB Performance

## 1. Designing Molecules Towards Low-Melting-Point or Liquid Forms

Pairing ORM with non-aqueous solvents in RFBs enables structural functionalization and utilization of a variety of electrolytes,<sup>1,6,21</sup> thereby offering possibilities in developing highly energy-dense systems. Because energy density is highly dependent on the concentration of active species (Eq. 1), developing ORMs with high solubility (> 1.0 M to be competitive with VRFBs) becomes critical for any commercially viable system. Another advantage of applying concentrated electrolytes is the ability to offset energy lost from molecule

tuning intermolecular interactions to develop ORMs with low-melting-point or ionic-liquid-form. Table 1 describes example ORMs that have been explored in this regard.

### 1.1. Pairing Non-Ionic ORMs/Solvent with Similar Polarity

For non-ionic ORMs, Van der Waals forces are the forces that cling them together. These intermolecular forces are the result of molecule polarity. Since a molecule is always surrounded by other molecules – either the same or different kind, the actual polarity of a molecule is a combined result of several contributing polar components. Therefore, molecules

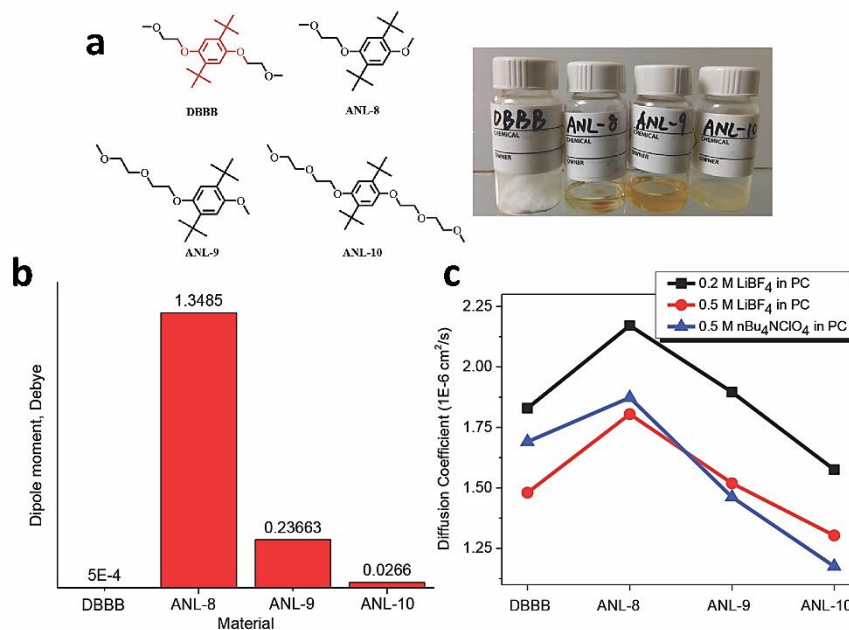


**Figure 1.** Illustration of tuning intramolecular dipole moments of 1,4-dimethoxybenzene (DMB) derivatives to obtain high solubility. (a) Structures (left) and physical states (right) of DMB derivatives studied. (b) Their corresponding dipole moments calculated by DFT. (c) Diffusion coefficient of the DMB species in various solvent systems. Reproduced with permission from ref. 40 Copyright © 2014 by John Wiley & Sons, Inc.

degradation. Therefore, we will begin with a discussion of efforts made in recent years to improve the solubility of electroactive materials.

Solvation, as a result of solvent-solute interactions, fundamentally relies on both the chemical and physical properties of solute (ORMs) and solvents. Understanding such interactions facilitates unraveling structure-property relationships, and may potentially develop universal strategies for improving solubility. Given that ORMs utilized are ionic and non-ionic compounds, approaches for tuning Van Der Waals forces and electrostatic forces of RFB systems will be described. Notably, considering that weakening molecular interactions lowers the energy required to break up solute compounds, preparation of ORMs towards low melting points or ionic-liquid-form is expected to be an effective approach to achieve high solubility. Further, once ORMs are liquid, they can function as a solvating medium. Liquid ionic ORMs also have the potential to be employed as supporting salts. Inspired by this analysis, the following section will detail strategies in

dissolving in each other is not only because their intermolecular forces are similar, but also because these composite forces are made up in a similar way. Such component interactions include dispersion forces, dipole-dipole forces, and hydrogen bonding (in the order of increasing strength). Consequently, solubility behavior will depend on (i) the result of intermolecular attractions in between, and (ii) the different types of polarities.

Non-ionic ORMs that have intrinsic weak intermolecular interactions (high symmetry, and small size) often possess high solubility in organic solvents as the solute-solute interactions are relatively easy to interrupt. Model ORMs that have been demonstrated in RFBs include 2,2,6,6-tetramethylpiperidine-1-oxyl (TEMPO),<sup>35</sup> 2,1,3-benzothiadiazole (BzNSN),<sup>36</sup> and Quinoxaline.<sup>37</sup> For example, Wei et al. applied TEMPO as a catholyte in a hybrid flow system, in which ethylene carbonate/propylene carbonate/ethyl methyl carbonate mixture (EC/PC/EMC) with LiPF<sub>6</sub> were employed as the supportive charge carrier.<sup>35</sup> In this

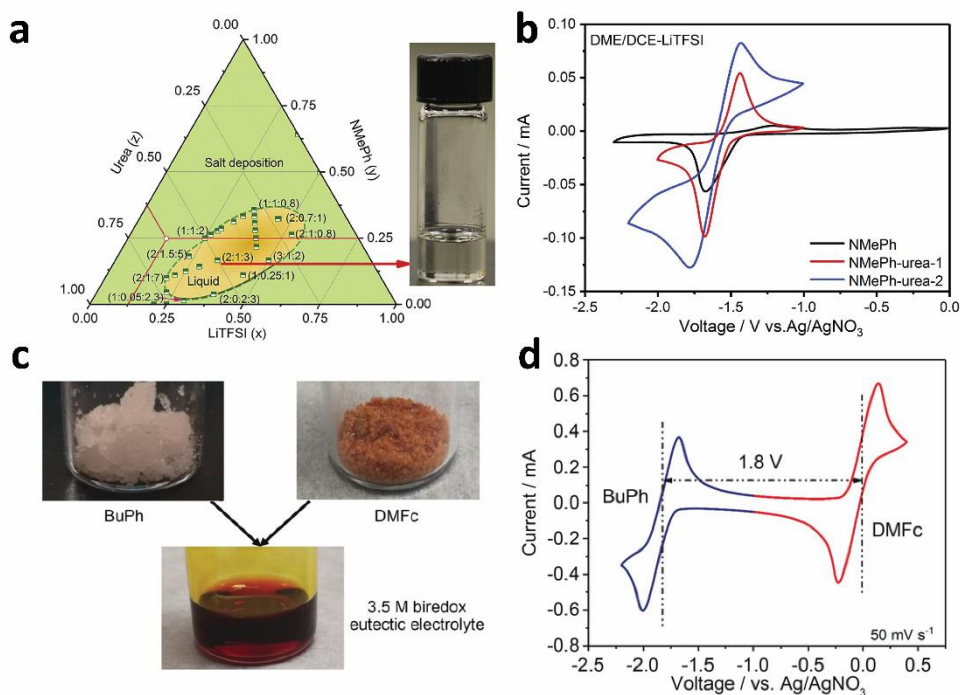


**Figure 2.** Strategies of applying deep eutectic solvent (DES) to prepare highly concentrate ROM liquids. **(a)** Phase diagram of the LiTFSI-NMePh-Urea system. **(b)** Cyclic voltammogram of NMePh in different solvents. Black line, 10 mM NMePh dissolved in 0.5 M LiTFSI/DME/DCE; red line, 10 mM NMePh with 0.03 M urea in 0.5 M LiTFSI/DME/DCE; blue line, 10 mM NMePh with 0.07 M urea in 0.5 M LiTFSI/DME/DCE. For all solvent systems, DME to DCE ratio is 3:1 (v/v). Scan rate, 50 mV/s. Reproduced with permission from ref. 44. Copyright, 2018, Elsevier Inc. **(c)** biredox DES composed of BuPh and DMFc. **(d)** Cyclic voltammogram of 50 mM DES with TBABF<sub>4</sub> added as supporting electrolyte. Scan rate, 50 mV/s. Reproduced with permission from ref. 45. Copyright © 2019 by John Wiley & Sons Inc

solvent system, TEMPO exhibited solubility up to 5.2 M in pure solvent, and 2.0 M with 2.3 M LiPF<sub>6</sub> added. Given this high concentration and cell voltage of 3.5 V, the TEMPO/Li system provided a volumetric energy density of 126 Wh L<sup>-1</sup>. A similar selection, BzNSN was reported by Dual et al.<sup>36</sup> BzNSN is highly soluble in organic solvents – 5.7 M in pure MeCN, and 2.1 M in 2.1 M LiTFSI/MeCN. Additionally, BzNSN possessed rapid electrochemical kinetics ( $k^0 = 0.9 \times 10^{-2} \text{ cm s}^{-1}$ ) and low redox potential (-1.58 V vs. Ag/Ag<sup>+</sup>), thus showing significant promise as an anolyte material. Cycling performance, however, is complicated by applying concentrated electrolyte. Increasing BzNSN concentration from 0.1 M to 0.5 M resulted in a dramatic increase in viscosity and crossover of electroactive species, which in turn, led to increased cell overpotential and poor current efficiency. The authors mitigated the impediments by decreasing charging current (from 60 to 10 mA cm<sup>-2</sup>), and replacing the 135  $\mu\text{m}$  thick Daramic separator with a 800  $\mu\text{m}$  thick membrane. Such modification has contributed to  $\sim 12\%$  increase in energy efficiency (EE). This viscosity and conductivity change as a function of concentration is a major challenge for employing concentrate electrolytes in NAQRFBs.

ORMs that have strong molecular interactions often suffer from low solubility in non-aqueous system. Note that for dissolution, the differences in solute-solvent polarity are

directly related to the degrees of intramolecular stickiness from one to another. Molecules that have similar polarities like to dissolve in each other. This occurs given the general rule that 'like dissolves like'. Since the dissolving medium utilized in NAQRFBs are often polar aprotic solvents (e.g., MeCN, DMF), functionalization of ORM by incorporating polar ether or ester groups to improve the intramolecular dipole moments have been proven to be effective in obtaining high solubility (Table 1).

Techniques to accomplish a high dipole moment of ORM through molecular pruning have been extensively documented by exploring 1,4-dimethoxybenzene (DMB) derivatives.<sup>38-40</sup> In a preliminary study, poly ethylene oxide (PEO) chain was introduced to prepare 2,5-di-tert-butyl-1,4-bis(2-methoxyethoxy)benzene (DBBB).<sup>38</sup> In comparison to 2,5-di-tert-butyl-1,4-dimethoxybenzene (DDB), the solubility of DBBB has improved 50-fold – 0.4 M in 'Gen 2 electrolyte' (1.2M LiPF<sub>6</sub> in carbonate ethylene carbonate (EC): ethyl methyl carbonate (EMC) with a 3:7 weight ratio). To further increase the solubility, attempts in altering PEO chain together with molecule symmetry was executed (Figure 1a).<sup>40</sup> Surprisingly, two of these molecules ANL8 and ANL9 were shown to be liquid at room temperature, suggesting much higher solubility than the DBBB base molecule and the possibility of a solvent-free RFB. It was also

found that the asymmetric nature of these molecules played a crucial role in increasing the dipole moments (Figure 1b) and lowering the viscosity, leading to high diffusion coefficients (Figure 1c). Importantly, these DMB derivatives retained the reversible electrochemical kinetics and high redox potential (around 4.0 V vs. Li/Li<sup>+</sup>), making them promising energy-dense catholyte molecules.

In subsequent studies targeted at maximizing gravimetric charge capacity, a subtractive approach was performed.<sup>39</sup> As presented in DBBB, the bulky *tert*-butyl groups and PEO chain could be potentially trimmed without sacrificing their electrochemical performance. Driven by the hypothesis, five derivatives were prepared. The results have shown that only 2,3-dimethyl-1,4-dimethoxybenzene (23DDB) and 2,5-dimethyl-1,4-dimethoxybenzene (25DDB) displayed good electrochemical reversibility. Conversely, the solubility of 23DDB and 25DDB were significantly enhanced – 2.0 M, and 0.6 M in 0.5 M LiTFSI/PC, respectively. Consequently, the molecular subtractive strategy has doubled the gravimetric capacities (161 mA h g<sup>-1</sup> for 23DDB, and 25DDB compared to 79 mA h g<sup>-1</sup> for DBBB).

The strategy of employing PEO chains to increase solubility in organic solvents was subsequently evidenced in phenothiazine species.<sup>41,46</sup> N-ethyl phenothiazine (EPT) is a promising catholyte due to its remarkable stability and relatively high redox potential (~0.3 V vs. Fc/Fc<sup>+</sup>). However, the low solubility (Table 1) impedes the practical implementation in RFBs. To address this, PEO chains of different length were incorporated via a one-step alkylation reaction.<sup>41</sup> In particular, N-[2-(2-methoxyethoxy)ethyl]phenothiazine (MEEPT) was discovered to be liquid at room temperature. Additionally, MEEPT showed stable cycling in a concentrated 0.5 M symmetric flow cell with relatively high charge/discharge currents near 100 mA cm<sup>-2</sup> and no detectable capacity fade. This capacity retention is remarkable in NAqORFBs. Of note, however, the reduced radical cation of MEEPT is only soluble up to 0.6 M, limiting the solubility of the material in actual application.

Further studies including PEO chains explored their use with ORMs including phenazines,<sup>47</sup> and quinones (e.g., benzoquinone (BQ),<sup>48</sup> 1,4-diaminoanthraquinone (DAAQ)<sup>42</sup>). These findings also revealed that the melting point of these materials could be significantly decreased when employing PEO chains. Such success yielded either highly soluble solids or liquid materials. It is also important to note that when designing ORMs for application in NAqORFBs, high solubility in the neutral state does not necessarily translate to high solubility in either reduced or oxidized form, and addition of supporting electrolytes decreases the solubility limits of ORMs in solution. Consequently, the solubility of charged states of ORMs with the presence of organic salts needs to be evaluated to select optimal operating conditions.

## 1.2. Developing Ionic ORMs with Low Lattice Energy

For ionic compounds, electrostatic forces become dominant in 'bonding' molecules together. Since the lattice energy reflects

the energy required to separate positive and counter ions, it can be used to indicate the solubility of a substance. In fact, solvent systems such as ionic liquids (ILs) and deep eutectic solvents (DESs), are based on the concept of decreasing lattice energy to enhance molecule solubility. These two strategies share the same principle – decrease the lattice energy by incorporating large, asymmetric ions, and thus decrease melting points. Different from ILs, which are a type of molecule that consists of discrete cations and anions, DESs are a mixture of Lewis or Brønsted acids and bases, i.e., a variety of anionic and/or cationic species are included.<sup>49</sup> Although transforming ORMs to room-temperature ionic liquids (RTILs) is attractive to improve energy density, it is often practically challenging. By contrast, DESs are prepared by simply mixing two or more components. As a result, there is a surge of interest in making DESs out of either catholyte or anolyte materials or both.<sup>50</sup>

An example in applying the strategy of eutectic electrolytes has been reported by Zhang et al. to improve the solubility of phthalimide derivatives (Figure 2a-b).<sup>50</sup> For example, N-methyl phthalimide (NMePh) exhibited low solubility (less than 0.7 M) in DME and DMF, but adding urea and LiTFSI lead to a significant improvement in solubility. Specifically, by tuning the LiTFSI/NMePh/urea molar ratio to 2:2:1.6, the concentration of NMePh reached ~ 4 M. Importantly, urea not only acted as a hydrogen bond donor, but also decreased the viscosity of this DES and promoted the reversibility of phthalimide radicals. The implementation of these eutectics was also shown to prepare a biredox DES – 1,1-dimethylferrocene (DMFc), and N-butylphthalimide (BuPh) were mixed together without any additional solvents (Figure 2c-d). This approach created the possibility of probing a high concentration symmetric NAqORFB wherein BuPh and DMFc were present at 3.5 M in a 1:1 molar ratio. By adding supporting salt to increase the conductivity of the solution, the concentration of these species decreased, but was effectively run in an RFB prototype at 1.0 M with a relatively high charging current of 60 mA cm<sup>-2</sup> as the viscosity remained low. Low coulombic efficiency was attributed to poor selectivity of the ion exchange membrane. As shown by these studies, the use of DES as anolyte, catholyte, or a combination of both is a viable solution to effectively increase the concentration of the electrolytes and thus promote a highly energy-dense NAqORFB.

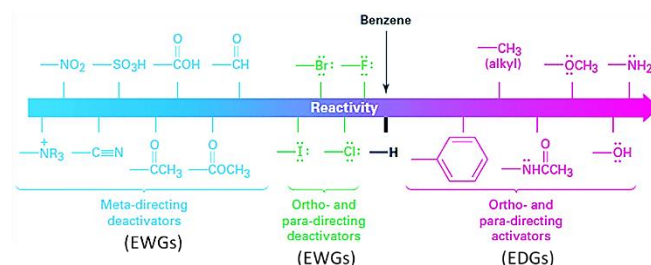


**Figure 3.** Classification of substituent effects. Reproduced with from J. E. McMurry, Organic Chemistry, Copyright 2012, Cengage Learning.

## 2. Powering Battery through Extending Redox Potential Gaps

Despite the advancements made in preparing electroactive species with high solubility, a caveat for operating RFBs at high concentrations is their changed dynamic properties. For NAqRFBs to be competitive with AqRFBs, flow cells need to be operational at electrolyte concentration over 1 M.<sup>51</sup> However, it has been reported that the ionic conductivities and ion diffusivities of redox-active monomers peak  $\sim 0.5$  M, and significantly decrease at higher concentrations.<sup>52</sup> The study of polymer kinetics also revealed that their diffusion-limited steady-state current reached a maximum (e.g., 0.6 M for 158 kDa, and 0.5 M for 318 kDa).<sup>53</sup> Further addition of polymers in supporting electrolytes led to the current decrease. These dynamic changes of ORMs as a response to high concentration suggests that merely targeting solubility of ORMs needs to be carefully re-examined. Another problem encountered in this regard is the possibility of increased crossover when using concentrated electrolytes.<sup>54</sup> Consequently, in order to achieve high power density, it is more preferable to increase the battery voltage and the number of electrons involved in redox chemistry. Given this analysis, we now turn our focus to research in extending cell voltage output and enabling multi-electron transfer.

The most widely applied approach in obtaining redox couples with a large potential difference is through structural

functionalization. Specifically, adding electron-withdrawing groups (EWG) or removing of electron-donating groups (EDG) increases electron affinity within ORMs, leading to a positive shift of redox potential; whereas incorporation of EDGs or subtraction of EWGs leads to a negative shift in redox potential. Figure 3 displays commonly used EDGs and EWGs in tuning battery voltage. In addition to this substituent effect, it is worth noting that salt environments can have a great impact on the redox potential of organic molecules. For example, cyclic voltammetry (CV) of 4-benzoylpyridinium derivative (**1**) was investigated in PF<sub>6</sub> salts with four different counterions.<sup>55</sup> Owing to the Lewis acidities of these cations, interactions with oxyanions (**1**) – the products of second electron cycling of **1**, resulted in a potential shift of **1**. This positive potential shift showed a linear response to the Lewis acidities of the salt cations (in the order of Li<sup>+</sup> > Na<sup>+</sup> > K<sup>+</sup> > TBA<sup>+</sup>). Compared to the half potential of **1** in TBAPF<sub>6</sub>, the value on the second electron cycling was 400 mV more positive when LiPF<sub>6</sub> was utilized. As such, tuning redox potentials by EDGs and EWGs has proved to be efficient, but the presence of electrolytes and solvents needs to be considered for accurate analysis.

Computationally, the substituent effects in aromatic molecules can be quantified by the Hammett constant  $\sigma$ .<sup>21,56</sup> For reactions with benzene rings involved, a Hammett constant describes the dependence of the equilibrium

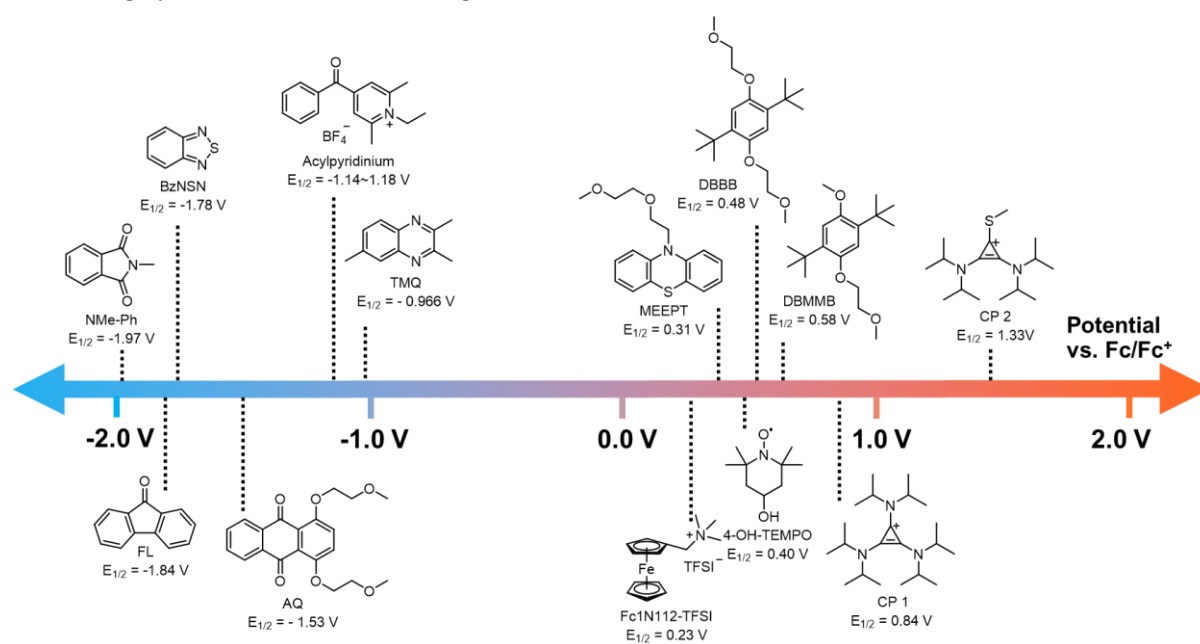


**Figure 4.** Summary of redox potentials of the state-of-art example ORMs studied in NAqRFBs. The chemical abbreviations associated with the references are listed as follows: NMe-Ph, N-methyl phthalimide;<sup>44</sup> FL, 9-fluorenone;<sup>26</sup> BzNSN, 2,1,3-benzothiadiazole;<sup>36</sup> AQ, anthraquinone derivative;<sup>63</sup> Acylpyridinium,<sup>1</sup> TMQ, 2,3,6-trimethylquinoxaline;<sup>37</sup> Fc1N112-TFSI, ferrocenylmethyl dimethyl ethyl ammonium bis(trifluoromethanesulfonyl)imide;<sup>1</sup> MEEPT, N-[2-(2-methoxyethoxy)ethyl]phenothiazine;<sup>41</sup> DBMMB, 2,5-di-tert-butyl-1-methoxy-4-[2'-methoxyethoxy]benzene;<sup>36</sup> 4-OH-TEMPO, 4-hydroxyl-2,2,6,6-tetra-methylpiperidine-1-oxyl;<sup>1</sup> DBBB, 2,5-Di-tert-butyl-1,4-bis(2-methoxyethoxy)benzene;<sup>37</sup> DBMMB, 2,5-di-tert-butyl-1-methoxy-4-[2'-methoxyethoxy]benzene;<sup>36</sup> CP1, N-(2,3-bis(diisopropylamino)cycloprop-2-en-1-ylidene)-N-isopropylpropan-2-aminium;<sup>64</sup> CP 2, 2,3-bis(diisopropylamino)-1-(methylthio)cycloprop-2-en-1-ylum.<sup>65</sup>

constants and rate constants of the reaction on the electron-donating or withdrawing substituents. The basic equation is as follows:<sup>56</sup>

$$\log \frac{K}{K_0} = \sigma \rho \quad (3)$$

Where  $K$  refers to the equilibrium constant with substituent (R), and  $K_0$  represents the equilibrium constant when R is a hydrogen atom.  $\sigma$  is the Hammett substituent constant, while  $\rho$  is the reaction constant that is independent on the substituents.

The ionization of benzoic acid or benzene carboxylic acid has been used to collect the Hammett substituent constant. Generally, EDGs destabilize the phenol anion, giving rise to negative Hammett constant; while EWGs stabilize the anion, resulting in positive Hammett's constant.<sup>57</sup> Further, the relative strength of electron donation or withdrawal is quantitatively described by the absolute value of this constant. For RFB applications, Hammett constant is employed to predict redox potential of ORMs since it is proportional to the Gibbs free energy change. Linear correlations between redox potentials and Hammett constant have been documented in ORMs such as in ferrocenes<sup>58</sup> and BODIPY Dyes.<sup>59</sup> The general trending is that EDGs possess negative Hammett constant, thus leading to a negative shift in redox potential. In contrast, EWGs cause a positive shift in redox potential, demonstrating the versatility of using Hammett constant in predicting redox properties. However, note that the way to tune catholyte with high oxidation potential *via* substituent effects requires the

incorporation of strong EWGs. This approach often leads to positive shifts of redox potentials. More importantly, the resultant cationic radicals, due to increased electron affinity, are more susceptible to reductive decomposition. For example, in the studies of over-charge protection of lithium-ion batteries, dimethoxybenzene containing an EWG of organophosphine oxide was prone to undergo reduction during discharge cycling.<sup>60</sup> A similar observation was also evidenced when phenothiazine was functionalized with chloride and bromide.<sup>61</sup> Consequently, catholytes incorporated with strong EWGs may possess high oxidation potentials, yet they may suffer from poor stability, leading to short cycling lifetime.

Alternatively, modification of redox potentials can be exploited by strain-induced disruptions of  $\pi$ -conjugated systems. A significant finding was reported by Casselman et. al using phenothiazine as a case study.<sup>62</sup> Typically for phenothiazine derivatives, the geometry of neutral ground state is bent, forming a 'butterfly angle', whereas the oxidized state tends to be planar. However, by adding EDGs (e.g., methyl, ethyl or isopropyl groups) in close proximity to the N substituent, the 'butterfly angle' of the radical cation was changed relative to their counterparts. i.e., the relaxation of the radical cation was disrupted. Accordingly, in contrast to the substituent effects, adding EDGs led to an increase of oxidation potential. Additionally, due to the elimination of EWGs, molecules often maintain good stability. This strain-induced modulation provides a paradigm shift in altering electrochemical properties. Nevertheless, the location of EDGs on the periphery of the fused-rings, along with their

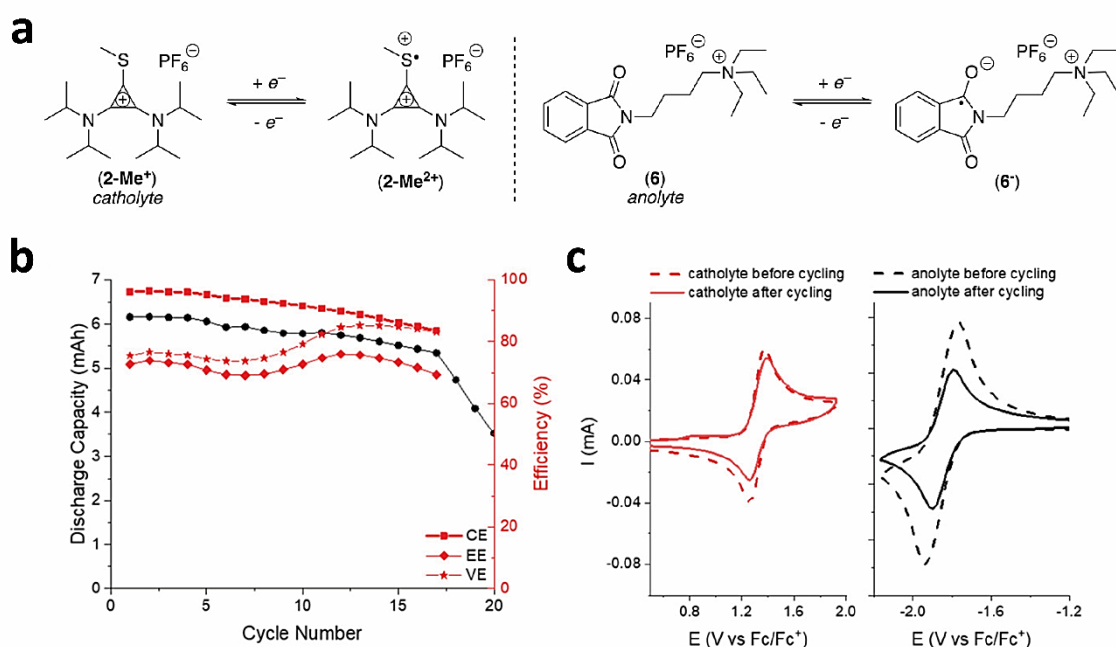


**Figure 5.** (a) An all-organic RFB with high cell output voltage (3.2 V) through pairing of cyclopropenium and phthalimide derivatives. (b) cycling performance of the 3.2 V flow battery. (c) Comparison of the Cyclic voltammetry of catholyte and anolyte before and after 30 cycles. (Image reproduced from ref. 65 with permission. Copyright 2019 American Chemical Society.)

structures, have been shown to have a great impact on the redox potentials as well as stabilities. Therefore, like substituent effects, the strain-induced approach also necessitates a thorough molecular screening and analysis to

When paired with a phthalimide derivative, 3.2 V cell voltage was for the first time achieved in all-organic RFBs. However, rapid capacity decay was observed after 17 cycles, and only 13% of the capacity was retained by 30 cycles. Further analysis

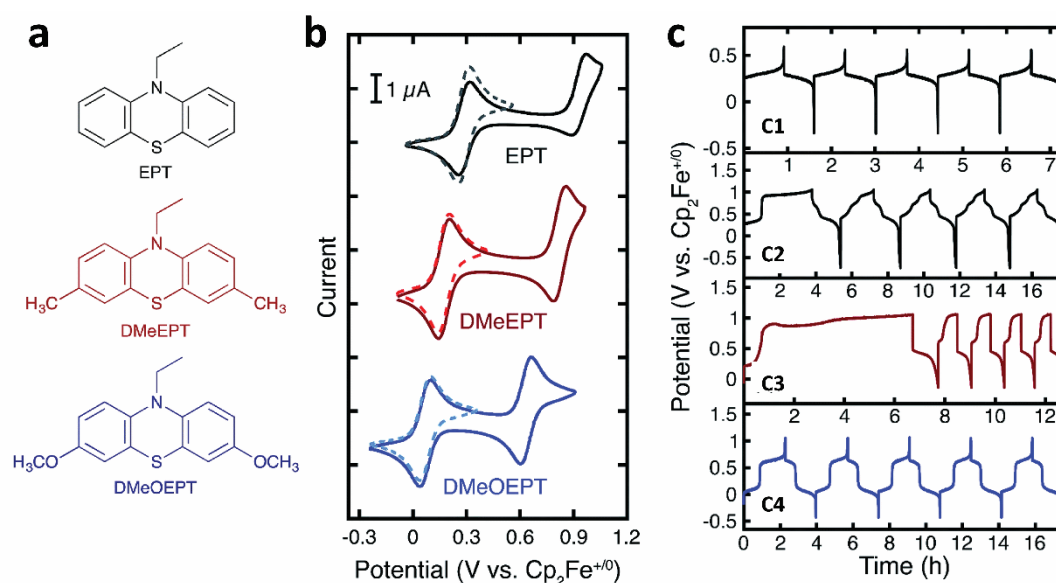


**Figure 6.** Molecular engineering of phenothiazine to develop two-electron-donating catholytes. **(a)** chemical structures of EPT (N-ethylphenothiazine), DMeEPT (N-ethyl-3,7-dimethylphenothiazine), and DMeOEPT (N-ethyl-3,7-dimethoxyphenothiazine). **(b)** CV analysis of the reversibility of the first and second electron transfer reactions. For all the experiments, 1 mM phenothiazine derivative was dissolved in 1 M LiTFSI/PC, and a scan rate of 10 mV/s was utilized. Dashed lines are the CVs with only first oxidation reaction, whereas solid lines include both oxidation events. **(c)** Cycling performance of charging/discharging phenothiazine derivatives, wherein C1, only cycling of first oxidation of EPT; C2 to C4 are the cycling of both oxidations of EPT, DMeEPT, and DMeOEPT, respectively. All experiments were conducted using 1 mM of electroactive catholytes in 1 M LiTFSI/PC solvent with a constant current of 0.804 mA applied. Images are reproduced from ref. 67.

prepare robust ORMs.

While molecular engineering through steric interactions effectively opens a viable pathway for tuning catholytes with high redox potentials without sacrificing good stability, the resultant redox potential is often within a narrow electrochemical window. For instance, adding two methyl groups for N-ethyl phenothiazine at the 1,9 positions (1,9-DMePT) led to a positive potential shift, but only with a change of 0.28 V.<sup>62</sup> Among all the ORMs developed, several anolytes with low redox potential close to -2.0 V vs. Fc/Fc<sup>+</sup> have been reported, while the redox potentials of catholytes are generally less than + 1.0 V vs. Fc/Fc<sup>+</sup> (Figure 4). As such, exploration of alternative catholytes that possess high redox potentials ( $\geq + 1.0$  V vs. Fc/Fc<sup>+</sup>) is demanding in order to realize high cell output voltage. Notably, cyclopropenium derivatives (CP) possess the highest oxidation potential to date, whereas phthalimides are the lowest reduction potential electrolytes. Sanford group has pioneered the study of pairing cyclopropenium salts with phthalimide derivative in RFBs.<sup>64</sup> Markedly, replacement of alkyl group with a weak  $\pi$ -donating sulfur substituent on CP resulted in a positive potential shift from 0.86 V to 1.33 V vs. Fc/Fc<sup>+</sup> in MeCN/TBAPF<sub>6</sub> (Figure 5).<sup>65</sup>

through CVs suggested that the degradation was primarily from the anolyte decomposition. Nevertheless, the work delivered an unprecedentedly high potential window (>3 V). Considering that the degradation mechanism of phthalimide was documented,<sup>43,66</sup> it is thus possible to further improve the battery stability by the engineering of phthalimide and solvent environment.

### 3. Access to Second Electron Transfer – Doubling Energy Density

Another route to improve energy density, as discussed in the previous section, is to employ chemical scaffolds that possess multi-electron transfer. Organic compounds offer a variety of candidates that fulfill this requirement. Utilization of these materials in flow batteries, however, present significant challenges. First, regardless of the presence of multiple oxidation states, the second redox events are often chemically or electrochemically irreversible. Second, cycling of highly charged states is often subject to rapid decomposition. Finally, such redox intermediates may suffer from poor solubilities as compared to their neutral states. Therefore, in the following discussion, we will describe approaches that address these demands to develop multi-electron storage ORMs. In

particular, we will highlight molecular engineering that enables reversible electrochemistry for high oxidation/reduction states.

Strategies to support multiple electron transfers have been demonstrated by the Odom group in screening phenothiazine derivatives.<sup>46,47</sup> Early work has shown that by incorporation of a polyethylene oxide (PEO) chain, the product MEEPT displayed enhanced solubility as compared to EPT.<sup>41</sup> Further efforts centered on substituents that enabled the simultaneous enhancement of solubility and reversibility of the second oxidation events, thus doubling RFB capability. The first attempt in this regard was to explore derivatization at positions *para* to nitrogen. As such, methyl and methoxy groups were anchored at the 3 and 7 positions of EPT, generating DMeEPT and DMeOEPT, respectively (Figure 6a). While both functional groups are EDGs, which could potentially stabilize the highly electron-deficient dication, methoxy groups can also delocalize charges by conjugation. Consistent with the hypothesis, cyclic voltammetry analysis (peak-to-peak separation, peak current ratio, and as a function of scan rate) indicated that the second oxidation event of DMeOEPT is more reversible than that of DMeEPT (Figure 6b). Although adding methoxy groups results in a negative potential shift, the ability to access to both electron transfers creates a net increase in energy density. Bulk electrolysis was subsequently performed to evaluate the long-term stability of DMeOEPT, with EPT and DMeEPT as comparisons. Figure 6c shows the potential profiles of the cycling performance. Specifically, **C1** depicts the charging/discharging of the first

for **C1**, and **C2** was 0.6 V, and 1.05 V (vs.  $\text{Cp}_2\text{Fe}^{+/0}$ ), respectively. **C3** and **C4** display the electrolysis performance of cycling DMeEPT and DMeOEPT with charging to 1.05 V vs.  $\text{Cp}_2\text{Fe}^{+/0}$ . The cycling performance indicates that (i) EPT is only stable for the first electron transfer. This stability is consistent with the CV analysis (Figure 6b). (ii) The prolonged charging process of DMeEPT suggested the formation of additional species as a result of the reductive decomposition of DMeEPT dication. The authors extended the electrolysis to 50 cycles. A stark contrast in the cyclic voltammograms before and after cycling was observed, which further confirmed the instability of DMeEPT. (iii) In contrast to EPT and DMeEPT, DMeOEPT showed constant voltage efficiency in the first five cycles. Even after 50 cycles, only 7% capacity decay was observed. Additionally, CV analysis of DMeOEPT before and after electrolysis indicated that active-molecule crossover, rather than dication degradation, attributed to this capacity fade. Consequently, the incorporation of EDGs and conjugation structure turns out to be a promising approach to develop two-electron electrolytes.

Despite the success, the extreme low solubility of DMeOEPT (<0.1 M for all states of charge in 1 M LiTFSI/PC) hinders its widespread application. Note that in the discussion of solubility, incorporation of ether group, the case in MEEPT, increases intramolecular dipole moment, and therefore greatly enhances solubility (Table 1). Accordingly, this strategy was employed to functionalize DMeOEPT to address its solubility issue.<sup>46</sup> Likewise, the replacement of short methoxy groups at the 3 and 7 positions with long oligoglycol chain was prepared

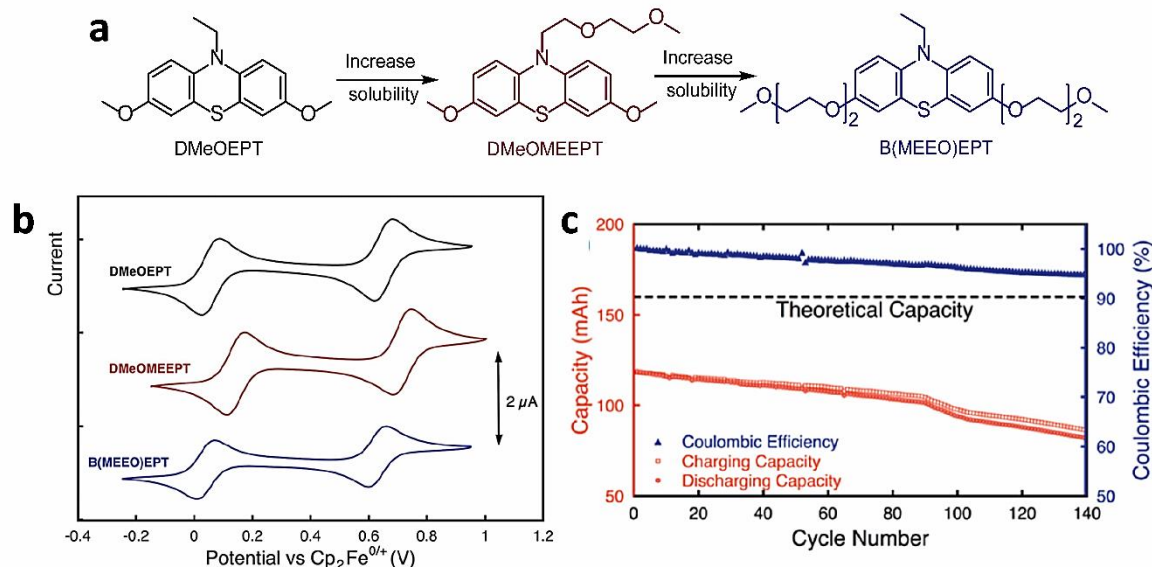


**Figure 7.** Strategies for increasing the solubility of two-electron-donating phenothiazines. (a) Illustration of pathways for synthesizing DMeOMEPT, and B(MEEO)EPT and their chemical structures. (b) CV analysis of the reversibility of DMeOEPT, DMeOMEPT, and B(MEEO)EPT. For all experiments, 1 mM of each phenothiazine was applied in 0.5 M TEATFSI/MeCN with a scan rate of 10 mV/s. (c) Cycling performance of B(MEEO)EPT in a symmetric flow cell configuration. Figure b and c are adapted with permission from ref. 46. Copyright 2019 American Chemical Society.

oxidation event of EPT, whereas **C2** shows access to both electron transfers. To achieve this, the cutoff voltage applied

(Figure 7a). DMeOMEPT and B(MEEO)EPT are both liquid at room temperature, indicating their neutral states can be

miscible in any ratio of polar organic solvents. The solubility of their radical cations and dications, however, displayed significant differences. For example, the radical cation of B(MEEO)EPT can be soluble up to 0.55 M in 0.5 M TEATFSI/MeCN system, while DMeOMEEPT is limited to 0.11 M. This solubility contrast is also reflected in the dications. Further evaluation also suggested that B(MEEO)EPT not only displayed superior performance in solubility, but also in reversibility (Figure 7b). In particular, the peak current ratio of the second oxidation reaction retained close to 1.0 for B(MEEO)EPT, whereas 0.9 was obtained for DMeOMEEPT. A current ratio of 1 is desirable as it signifies chemical reversibility. Accordingly, B(MEEO)EPT was selected for flow cell experiments (Figure 7c). Importantly, the charging/discharging process was investigated with symmetric cell setup<sup>41</sup> – a cell configuration similar to VRFBs. By applying 0.3 M B(MEEO)EPT and constant current at 25 mA cm<sup>-2</sup>, 80% of capacity could be accessed initially. However, 27% of the capacity loss was observed after 140 cycles. Interestingly, evaluation of cell components through microelectrode voltammetry and UV-vis absorption spectroscopy indicated that this fade was not due to the decomposition of electroactive species (e.g., B(MEEO)EPT, B(MEEO)EPT<sup>•+</sup>, or B(MEEO)EPT<sup>2+</sup>). Nevertheless, a potential pitfall of employing such symmetric cell cycling is the formation of an imbalanced cell *via* disproportionation reaction of dication and neutral species. Such a mismatch in the concentration of active species may alter potential profile, which in turn, limits the capacity that can be potentially accessed.

The results of functionalizing of EPT to DMeOEPT and DMeOMEEPT suggests the ‘dual’ function of incorporating conjugated EDGs – simultaneous enhancement of solubility and reversibility, in particular for the second electron transfer events. In fact, studies of DAAQ derivatives reveal a similar principle. DAAQ possesses five oxidation states, but irreversible reactions were observed for both high oxidation states.<sup>68</sup> Simple substitution of a proton in the amino group (–NH<sub>2</sub>) with a methyl group (–NHCH<sub>3</sub>), however, enabled reversible oxidations. Similar to DMeOEPT, the solubility of the methyl-substituted DAAQ (NMe-DAAQ) is poor (Table 1). This solubility challenge was again addressed by incorporation of polar PEO chain.<sup>42</sup> The similarity in molecular engineering of phenothiazine and DAAQ indicates that conjugated EDGs are advantageous over simple EDGs in improving electrochemical performance. Although this analysis alone does not provide a definitive description of obtaining two-electron-donating redox-active species with high solubility, there is clear evidence that this approach might also be applicable to other ORMs.

Metal coordination complexes (MCCs) are another class of promising redox-active molecules that exhibit multiple oxidation states through redox events of the metal and/or ligands. Similar to the aforementioned ORMs, MCCs are capable of functionalization *via* molecular engineering of their organic components – the ligands. For instance, for the cobalt (II) terpyridine complex ([Co(tpy)<sub>2</sub>]<sup>2+</sup>), the replacement of one pyridine with an electron-deficient 1,2,4-triazole resulted in

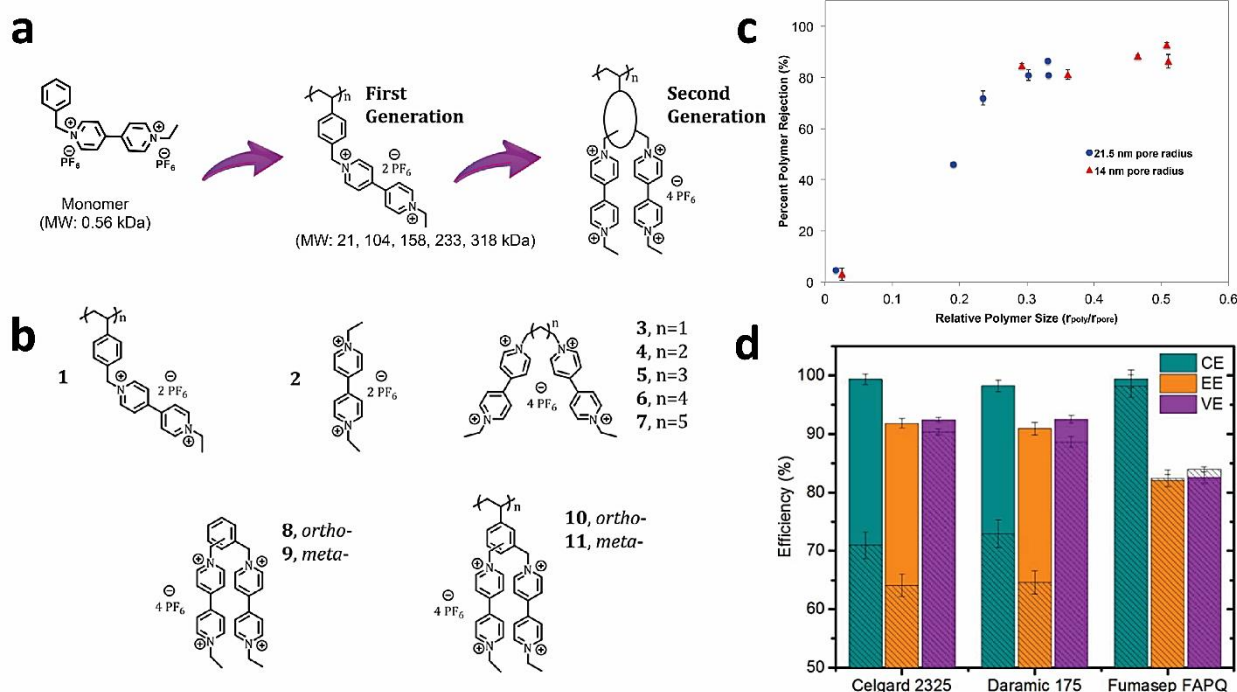


**Figure 8.** Evaluation of the structural effects of viologen on the active-molecule crossover performance. (a) schematic illustration of molecular engineering of viologen-based molecules. (b) Structures of monomers, dimers, and polymers evaluated to uncover their differences in electrochemical properties. (c) Crossover performance as a function of relative polymer size. The images a–c were adapted with permission from ref. 53 Copyright 2014, and 78 Copyright 2016, American Chemical Society. (d) Battery performance of RAP (solid) and monomers (line) in coulombic efficiency (CE), energy efficiency (EE) and voltage efficiency (VE) when IEMs and porous membranes were used. Reproduced from ref. 79 Copyright 2017 The Electrochemical Society.

positive potential shifts for both Co(II/I) and Co(III/II) couples.<sup>69</sup> Accordingly, the cell voltage increased from 1.07 V to 1.50 V. When two pyridine groups were substituted by weaker  $\sigma$ -donating/ $\pi$ -accepting 3,5-dimethylpyrazole, the redox potential difference of the cobalt couples were further increased to 1.91 V.<sup>69</sup> Additionally, solubility of MCCs can also be tuned through the incorporation of polar ester groups. In the studies of Cr and V acetylacetonate (acac) complexes, for example, Suttill et al. have demonstrated that acac ligands bearing with 2-methoxyethyl substituted ester showed solubilities of 1.8 M, and 1.3 M for Cr and V centers, respectively. These solubilities are about  $\sim$  3-fold improvement

complexes for non-aqueous redox flow batteries'.<sup>71</sup> Advancements made in employing MCCs in non-aqueous redox flow batteries have also been recently reviewed elsewhere.<sup>72</sup>

A more relevant to the topic of stabilization of second electron transfer is the gravimetric capacity. Although molecular functionalization often results in an increase of molecular weight of ORMs, the ability to access the second electron can compensate for this increase, leading to a further improvement of gravimetric capacity and energy density. In the studies of phenothiazine derivatives, for example, DMeOEPT is 26% larger than the parent molecule EPT.

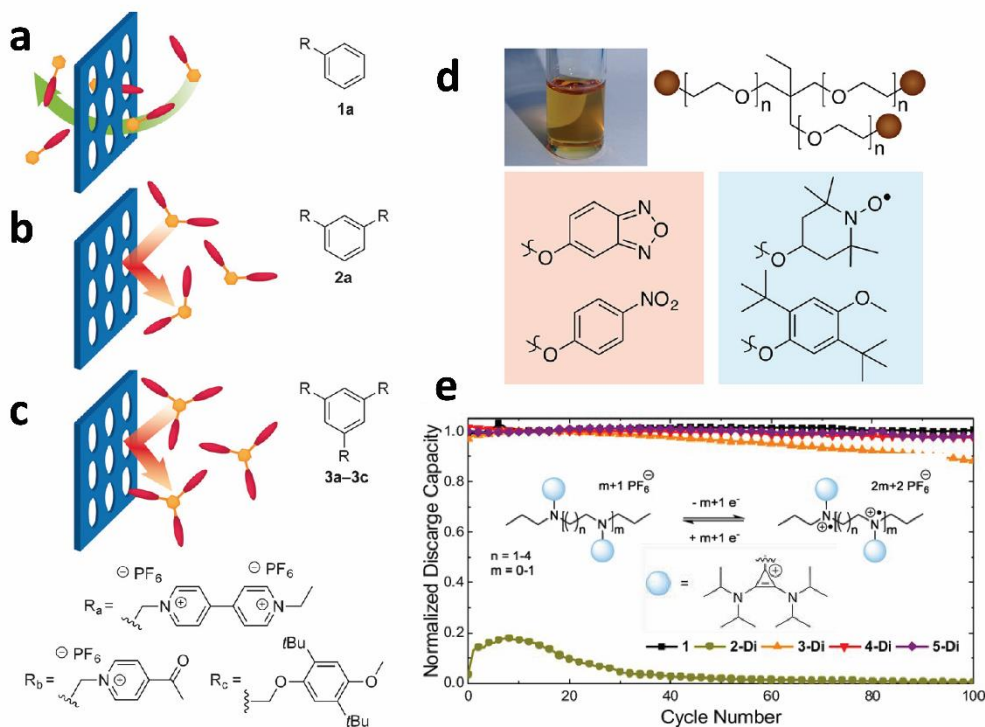


**Figure 9.** Examples of applying redox-active oligomers (RAOs) with PIM membranes to resolve crossover. (a-c) Illustration of macromolecular design in mitigating active-species crossover. Reproduced with permission from ref. 82. (d) Incorporation of oligoethylene oxides as core motifs with various redox centers produces liquid RAOs. Reproduced with permission from ref. 81 Copyright, 2018, American Chemical Society. (e) The impact of carbon spacer on the cycling performance of CP oligomers. Adapted from ref. 83 Copyright 2018 American Chemical Society.

compared to that of their parent Cr(acac)<sub>3</sub> and V(acac)<sub>3</sub> complexes.<sup>70</sup> Such functionalization in redox potential and solubility indicate that there are similarities present in engineering ORMs and MCCs.

However, unlike ORMs that are solely composed of organic moieties, the metal components in MCCs also play a critical role in their properties. In fact, it has been reported that the choice of the metals has a significant impact on the electrochemistry of MCCs, including their redox potentials and chemical reversibility.<sup>71</sup> Due to the focus of the current review is ORMs, it is beyond the scope to summarize the effects of a variety of metal centers on MCCs properties and battery performance. For more information on this topic, please see 'Structure-function relationships of metal coordination

However, *via* stabilized dications, the molecular gravimetric capacity was improved to 187 Ah kg<sup>-1</sup> – a 58% increase of the gravimetric capacity.<sup>67</sup> Other attempts in this regard have been reported, including minimization of the molecular weight of ORMs (e.g., dimethoxybenzene-based redox materials<sup>39,73</sup>), and replacement of bulky cations with small ions to facilitate ionic coupling between ORMs and supporting electrolytes.<sup>74</sup> A potential caveat is that such modification in the battery system may result in poor cycling stability. This is especially the case when a subtractive approach is applied.<sup>39</sup> Consequently, to achieve optimal performance of NAQRFBs, all parameters that are associated with power density and energy density need to be considered for optimization.

#### 4. Minimizing Redox-Molecule Crossover for High Current Efficiency

Although operation of RFBs in a non-aqueous environment offers considerable chemical and structural versatility in electroactive materials and large electrochemical window (~5 V), adapting commonly applied ion exchange membranes (IEMs) from aqueous to non-aqueous regime brings in another significant challenge. This is due to the fact that most widely used IEMs such as Nafion are proton conductors. As such, utilization of these IEMs in organic solvents leads to a significant decrease of ionic conductivity to only 0.2-0.5 mS/cm – roughly an order of magnitude lower than that of in an aqueous setup.<sup>34</sup> Accordingly, the low ion conductivity observed in non-aqueous electrolytes places limits on the power density that could potentially be achieved in NAqORFBs. Together with the issue of the high cost of IEMs, the development of alternative membrane materials becomes imperative.

##### 4.1. Redox-Active Polymers (RAPs)

Hydrocarbon polymer-based microporous separators, including Deramic and Celgard are cheap and exhibit high ionic conductivity in organic solutions. However, their large pore radius (typically ~ 10-20 nm) imperils crossover of redox-active species. To address this issue, redox-active polymers (RAPs) pairing with size-exclusion membranes have been developed.<sup>34</sup> Examples include TEMPO-crowded bottlebrush polymers,<sup>75</sup> poly(boron-dipyrromethene),<sup>76</sup> phthalimide-containing,<sup>66</sup> and Cyclopropenium RAPs.<sup>77</sup> Importantly, the Rodríguez-López group pioneered the study of systematic molecular design of viologen-based RAPs (Figure 8),<sup>53,78,79</sup> leading to significant findings, namely: (i) a strong correlation between the polymer molecular weight and pore size on the RAP crossover has been observed (Figure 8a). With the RAPs possessing high molecular weight (M.W.  $\geq 158$  kDa), commercially available separators (pore size  $\geq 14$  nm) showed ca. 70 times higher selectivity for LiBF<sub>4</sub> in comparison to RAPs. Further analysis suggested that when the relative polymer size increased to 0.3, over 80% of rejection of active species could be achieved (Figure 8b).<sup>78</sup> This high rejection rate demonstrates the feasibility of using size-selective separator aided by RAPs to prevent the crossover of electroactive species in NAqORFBs. (ii) Subsequent investigations of molecular engineering suggested that structural variations in spacer length and moieties gave rise to distinct electrochemical properties for dimers and their corresponding RAPs (Figure 8c).<sup>21</sup> For example, the alkyl chain length in the dimers plays a crucial role in self-exchange reactions, which in turn impacts their kinetics. Although dimer 8 displayed good reversibility and high coulombic efficiency, translation of 8 to a polymer 10, however, resulted in irreversible redox chemistry. Conversely, increasing the rigid length from *ortho*- to *meta*-position reversed the observed

polymer properties – the half cycles in polymer 11 were symmetric and Coulombic efficiency was above 90% with over six cycles. The observed disparity potentially results from the fact that the charge transport within RAPs' inner bulk is three-dimensional, and in response to polymer dynamics. (iii) Despite the complexity revealed in engineering RAPs, the high selectivity achieved by RFBs utilizing RAPs was further evaluated with Celgard 2325 and Daramic 175 as a comparison to the IEM Fumasep FAPQ in a flow cell configuration.<sup>79</sup> When Fumasep was applied as the separator, similar Coulombic efficiencies (CE) were observed for monomers and polymers. By contrast, in the frame of porous membranes, polymers demonstrated better performance with high CE over monomers (Figure 8d).<sup>80</sup> These results evidenced the impact of pairing RAPs with porous membranes in prevention of material crossover. In addition, it is important to note that the RAPs prepared also possess high solubility – as high as 1.0 M in acetonitrile, indicating their great potential in attaining high energy density. Nevertheless, a caveat for applying RAPs in NAqRFBs is their sluggish mass transport, which is typically 2 orders of magnitude lower than their monomers.<sup>81</sup> Consequently, the strategy using RAPs with porous membranes is effective in controlling crossover, but the complexity in structure-property relationships acquires rigorous molecule screening to disclose the optimum compositions of RAPs.

##### 4.2. Redox-Active Oligomers (RAOs)

In line with RAPs, ion-selective membranes derived

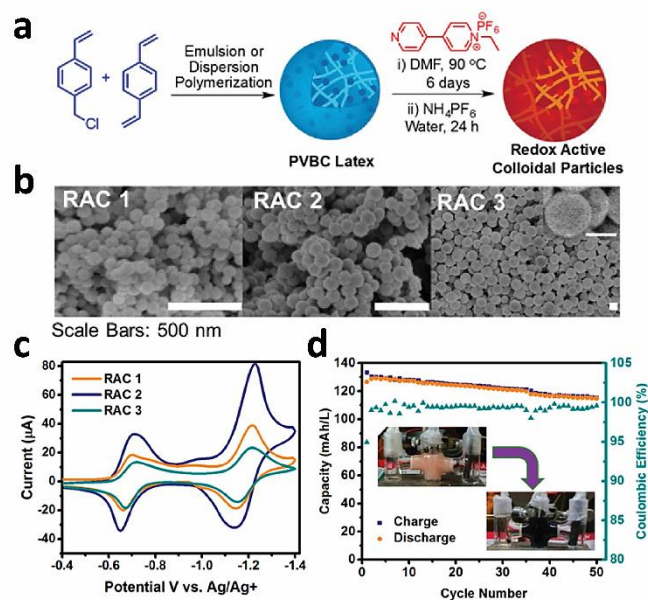


**Figure 10.** Preparation and performance of bipyridine-based redox-active colloids (RACs). (a) Synthetic procedures for RACs with a wide range of size. (b) SEM images of the produced RACs. From RAC1 to RACs, the particle diameter was  $80 \pm 11$ ,  $135 \pm 12$ , and  $827 \pm 71$  nm, respectively. (c) Cyclic voltammetry (CV) of 10 mM RACs in 0.1 M LiBF<sub>4</sub>/MeCN solution. All the CVs were recorded using 3 mm<sup>2</sup> Pt disk electrode with scan rate of 75 mV/s. Adapted with permission from ref. 84. Copyright 2016 American Chemical Society.

from polymers of intrinsic microporosity (PIMs) were documented in mitigating active-material crossover.<sup>82</sup> Unlike Celgard and Daramic, separators derived from PIMs feature pore size less than 1 nm, thus enabling smaller molecules such as redox-active oligomers (RAOs) to be employed. One important advantage of RAOs is their facile charge transport – about one order magnitude higher than that of RAPs.<sup>81</sup> On the other hand, the decrease in membrane pore size only lowers membrane ionic conductivity from 2.2 mS/cm to ~0.4 mS/cm, while the blocking ability was significantly improved. For example, even for the monomers **1a**, replacement of Celgard with PIM-1 gave rise to a 40-fold improvement in crossover prevention. This blocking ability was further enhanced after chemically cross-linking of PIM-1, which impeded pore swelling in the electrolyte. The performance of the aforementioned membranes in managing active-species crossover is summarized in Table 2, and the chemical structures are displayed in Figure 9a-c. The success in pairing PIM-1 with RAOs indicates the great potential of this strategy in enhancing NAqRFB performance. Inspired by the study, RAOs with a variety of redox centers were also prepared.<sup>81</sup> Importantly, the use of oligoethylene oxides as core motifs transformed RAOs to be liquid, allowing the battery to attain high volumetric capacity (Figure 9d). Molecular screening of RAOs with tris(dialkylamino)cyclopropenium suggested the impact of oligomer size and structure (e.g., link spacer, the number of redox centers on each individual RAO) on their electrochemical properties (Figure 9e).<sup>83</sup> Collectively, these investigations lay the foundation for battery principles in which the size-exclusion effect is dominant for preventing ORM crossover.

**Table 2.** Comparison of the membrane blocking ability using PIM membranes and traditional porous membrane Celgard. The blocking ability was derived from the ratio of the diffusion coefficient of each molecule through the membrane ( $D_{\text{eff}}$ ) to its diffusion coefficient through solution ( $D_{\text{sol}}$ ). Adapted from the Ref. 82.

Redoxmers	ROA size (Å)	Celgard	PIM-1	Cross-linked PIM-1
Monomer <b>1a</b>	8.8	30	1,280	14,200
Dimer <b>2a</b>	12.3	30	11,600	297,000
Trimer <b>3a</b>	16.8	30	32,900	85,000

#### 4.3. Redox-Active Colloids (RACs)

Note that the key to controlling material crossover using RAPs is to achieve a good balance between the polymer size and the pore size of the selective membrane. While it is possible to control the size of RAPs by polymerization, the possible range obtained is limited. The preparation of membranes with a variety of pore radii is another approach, but this can be tedious and only applicable to specific molecule sizes. Given this consideration, Montoto et al. introduced an alternative approach in which redox-active colloids (RACs) were synthesized (Figure 10).<sup>84</sup> The key advantage of RACs, in comparison to RAPs, is the wide range of colloid size that can

be potentially obtained. Because RACs are spherical particles with cross-linked polymer chains incorporated within, their size after polymerization can be spanned from tens to thousands of nanometers. Three viologen-based RACs were prepared with particle diameters of  $80 \pm 11$ ,  $135 \pm 12$ , and  $827 \pm 71$  nm, respectively (Figure 10a-b). Cycling of these RACs using separator Celgard 2325 exhibited near-zero crossover, and 99% CE over 50 full cycles (Figure 10d). Notably, effective electron transfer within RACs was observed regardless of their size (Figure 10c). In principle, the crosslinked nature of RACs sets a large degree of structural rigidity within the colloid, thus imposing the necessities of long-distance electron transfer. This efficient long-distance intraparticle charge transfer might be a result of their increased surface area as well as particle swelling, which promotes the diffusion of counterions. The strategy demonstrated here opens up an avenue to prepare RACs with other versatile redox functional groups. A follow up study through single particle measurements and Raman analysis enabled the exploration of the impact of individual RACs on cycling performance.<sup>85</sup> This investigation indicated that RACs with smaller sizes (< 830 nm) and unravel of key structure-property relationships may improve electron transfer and charge transfer within colloids. As a result, it is suggested that to expand the application of RACs in NAqORFBs, a thorough understanding of their charge transport and cycling performance as a response to the morphology and structures, are of importance.

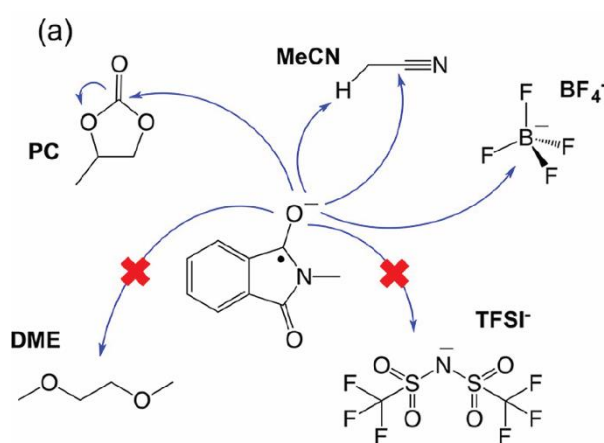
#### 4.4. Other Alternative Approaches for Addressing ORM Crossover

With the surge of interest in porous membranes aided by macromolecule engineering to improve crossover resistance, research in exploring other alternative strategies is flourishing. Very recently, Paula et al. have innovated a membrane-free battery model. In such a system, redox-active molecules are dissolved in two immiscible electrolytes, forming a biphasic electrochemical cell. Unlike microfluidic redox flow batteries in which the elimination of membrane is achieved by laminar flow, this battery takes advantage of immiscibility so that the electrolyte volume is not limited in a confined microchannel. A proof-of-concept battery was prepared by employing two quinone species in an ionic liquid phase and a hydrochloric acid solution as catholyte and anolyte, respectively.<sup>86</sup> This approach was further expanded to organic solvents (e.g., butanone and propylene carbonate) and other electroactive molecules (e.g., TEMPO derivatives, and anthraquinones).<sup>87</sup> Optimal battery composition showed ~ 75% Coulombic efficiency for over 300 cycles, underlining its great potential in NAqORFBs. However, owing to the lack of membrane, cross-migration driven by thermodynamics can result in an imbalance of active molecules (e.g., high potential molecules migrate to the side with low potential species) and battery self-discharge. Although the partition coefficient was measured for analyzing the crossover effect, it is important to note that no flow was applied for all the testing. As the feasibility of the membrane-free approach has been

demonstrated on a technical level, future efforts in understanding the system, in particular, partitioning of redoxmers in two phases under different flow rates, are critical.

Another emerging research development is the utilization of one single redox couple or bipolar redoxmers (BRDs). Unlike the aforementioned molecules, BRDs possess the redox moieties needed for both the positive and negative half-reactions, thus leading to identical electrolyte components in catholyte and anolyte compartments.<sup>68</sup> As such, the physical crossover of BRDs does not cause mixing of disparate species. The key advantage of this 'symmetric' design is that the battery 'self-balances' to counteract the capacity loss as a result of active-molecule crossover. BRDs bearing a large variety of redox centers<sup>54,88-92</sup> have been prepared and investigated in the flow battery system, highlighting new opportunities in mitigating active-species crossover in RFBs. This strategy, together with size-selective separators aided by macromolecules, have established the fundamentals to approaching high CE and long cycling lifetime. Considering the limited molecular engineering reported in BRDs and macromolecules, it is thus possible, in principle, to further improve crossover performance while attaining high power density in NAqORFBs using this strategy.

### 5. Enhancing Molecule Stability – Application to Long-Serving Batteries



chemical species.<sup>93</sup> These radicals may react with other ORMs (most likely in desirable high-concentration systems given frequent ROM association), solvents, and supporting electrolytes and subsequently negatively affect the energy density of the NAqORFBs.<sup>26,94</sup> Thus, in this section, we will discuss recent efforts made in elucidating possible decomposition pathways of ORMs to advance the stability and cycling lifetime.

Considering that chemical conditions often play a vital role in electrolyte shelf-life, optimization of the operating environment, such as the choice of solvent system, must be carefully examined. The impact of solvents and salts on cycling lifetime has been well-documented in organic carbonyl compounds (OCCs). OCCs, as a subgroup of ORMs developed, have been extensively studied in the past decade owing to their high capacity, low cost, and structural diversity.<sup>10,22</sup> In particular, there is a surge of interest in imides including fluorenone (FL)<sup>26,47,95</sup> and phthalimides (Ph).<sup>43,44,96</sup> Their extremely low redox potentials ( $< -1.7$  V vs.  $\text{Ag}/\text{Ag}^+$ ) of FL and Ph stretch the research boundary to develop highly energy-dense systems (Figure 5). The reduced active species – ketyl radical anions ( $\text{FL}^{\bullet-}$  and  $\text{Ph}^{\bullet-}$ ), however, are electrophilic and susceptible to nucleophilic attack to any electron-deficient molecules present in the system. Consequently, unsuitable electrolyte composition can be disastrous to cycling performance. For instance, Wei et al. has reported pairing of

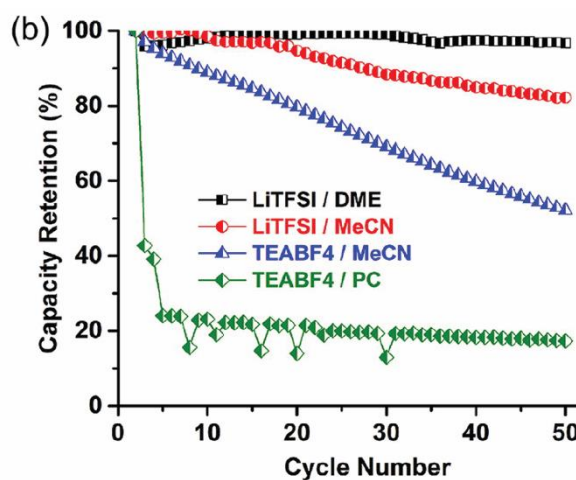


**Figure 11.** Illustration of the impact of solvents and salts on the NMePh cycling lifetime. (a) Plausible degradation mechanisms of NMePh. The electrophilic nature of  $\text{MePh}^{\bullet+}$  results in reactions with electron-deficient molecules (PC, MeCN,  $\text{BF}_4^-$ ), whereas  $\text{MePh}^{\bullet-}$  is stable in LiTFSI and DME. (b) Cycling performance of using MePh and DBMMB as anolyte and catholyte, respectively. For all experiments, 0.1 M electrolytes were utilized, and a constant current density of  $10 \text{ mA cm}^{-2}$  was applied. Produced with permission from ref. 43. Copyright 2016 American Chemical Society.

Finally, it is imperative to address the stability of ORMs in RFBs as the commercialization of NAqORFBs will require the long-term cycling of these ORMs through over 10,000 cycles. The difficulty arises, however, because charging and discharging of ORMs generates radical species with unpaired electrons, which are generally more reactive than the initial

N-methyl phthalimide (NMePh) and 2,5-di-tert-butyl-1-methoxy-4-[2'-methoxyethoxy]benzene (DBMMB) in flow battery.<sup>43</sup> Similar to FL,<sup>26</sup> solvents and salts have shown to be vital in the charging/discharging process (Figure 11). When tetrafluoroborates, MeCN, and carbonates were employed, their electron-deficient functionalities rapidly deactivated

MePh<sup>-</sup>. Accordingly, a combination of MeCN and TEABF<sub>4</sub> resulted in the least stable cell. Conversely, the application of LiTFSI and DME afforded constant capacity over 50 cycles owing to the absence of electron-deficient elements. While degradation mechanisms of ORMs may vary, these results highlight the necessity for a rigorous selection of solvent systems to improve cycling lifetime.

These results of studying OCCs has revealed that ORM stability in RFBs is typically limited by the radical state, which is generally the least stable. Therefore, gaining an understanding of parameters affecting the charge dispersion/localization and steric protection is vital for developing persistent ORMs. This may be accomplished through the derivatization of a redox-

decay *via* protonation.<sup>98</sup> Considering the lower pK<sub>a</sub> of ketone enolate anions (26.5 for acetone and ethyl acetate, and 29.5 for ester enolates), acetylpyridinium salt (**Py2**) was prepared. Improved stability was evidenced in the CV analysis in LiBF<sub>4</sub>/PC solvent, in which **Py2** showed reversible redox couples (Figure 12b-ii), whereas **Py1** exhibited significant decomposition (Figure 12a-ii). Further attempts to extend the radical shelf-life was performed by developing 4-benzoyl-N-(2,6-dimethylphenyl) pyridinium (**Py3**) (Figure 12c-d).<sup>99</sup> It was noted that steric bulk around the nitrogen group distal from the radical carbon upon charging shared a positive correlation with radical persistence. However, by simply substituting the nitrogen with bulky groups (i.e. phenyl and tertbutyl), the E<sub>1/2</sub>

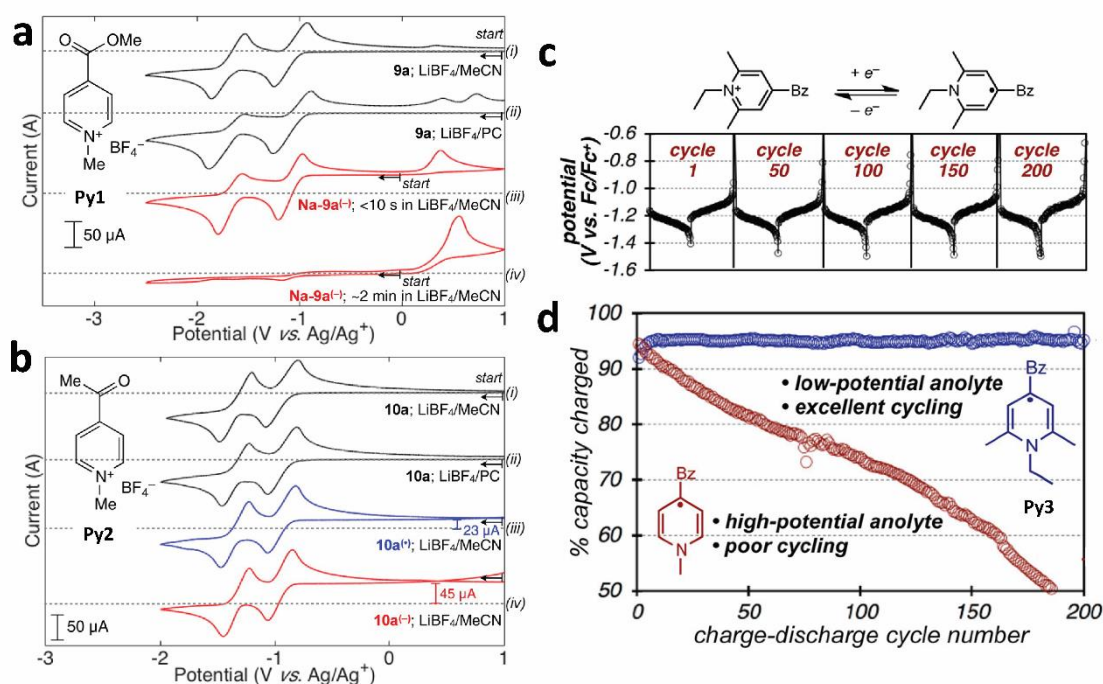


**Figure 12.** (a-b) CV analysis of **Py1** and **Py2** in different solvent systems. For all experiments, 0.01 M of electrolytes was dissolved in 0.1 M LiBF<sub>4</sub> with specified solvents as indicated. Scan rate, 100 mV/s. (c) Selected potential profiles during cycling of **Py3**. (d) Comparison of cycling performance of two benzyl pyridinium derivatives. Adapted with permission from ref. 99. Copyright 2017 American Chemical Society.

active base molecule and subsequent modelling for extrapolation of molecular stability. Various groups have modulated stability of ORMs through chemical intuition and understanding of decomposition pathways.<sup>39,46,73,83,97</sup> This allows for the synthesis of more stable ORMs, but modelling and gaining an understanding of specific, quantitative contributions allows for more precise tuning of molecular stability in many cases without compromising desirable ORM characteristics such as high solubility, high or low potential, and so forth. Notably, the Sandford and Sigma groups have pioneered applying this statistical modeling in developing stable pyridinium derivatives.<sup>98,99</sup> The early study of N-alkyl pyridinium indicated that the incorporation of highly basic functional groups such as ester enolates (**Py1**) led to rapid

values of the molecules were inversely affected. Through chemical intuition, a parameter was generated which described the height out of the plane ( $h_{st}$ ), which positively correlated to molecular stability. Through the use of this parameter combined with E<sub>1/2</sub> values, these researchers were able to isolate highly persistent radicals through extrapolation, which demonstrated stable cycling through 200 charge/discharge cycles while the parent pyridinium compound experienced a 35% capacity fade in the same conditions.

In a subsequent study, the same groups have sought to increase the potential of cyclopropenium while attaining good stability.<sup>100</sup> Cyclopropenium, as shown in Figure 4, possess high redox potential, and thereby is a promising candidate for RFB

applications. After understanding symmetry and charge delocalization, they successfully predicted that by disrupting this symmetry through substitution of a thio group in place of one of the nitrogen groups the potential would drastically increase.<sup>101</sup> However, after synthesis of the thio-cyclopropenium derivative, it showed irreversible electrochemistry. Subsequent analysis of the decomposition pathway showed the C-S bond cleavage and the presence of a tertbutyl carbocation. This knowledge allowed for the computation of more stable derivatives through decreasing the NBO charge at the carbon  $\alpha$  to the sulfur atom *via* alkyl substitution without detrimental effects to the desirable  $E_{1/2}$  values (around 1.4 V vs. Fc/Fc<sup>+</sup>). The computed molecules showed reversible electrochemical behavior and the cyclopropenium containing a methyl substituted thio group exhibited stable cycling through 150 cycles with greater than 98% Coulombic efficiency.

As shown by these studies, with quantitative understanding of both steric and electronic parameters that affect the electrochemical stability of electrolyte materials, these may successfully be modulated to increase cycling stability. Importantly, it has been demonstrated that this may be accomplished without detrimentally affecting properties of interest. Statistical modeling and computational chemistry thus provide the most promising pathway forward to discover ORMs with high stability for application in NAqORFBs.<sup>102</sup>

### III. Challenges and Immerging Needs

In order to address the challenges associated with developing high-performing ORMs for application in NAqORFBs, it will be necessary to understand fundamentals associated with stability, solubility, charge, crossover, and the modulation of redox potentials to maximize the utilization of organic solvent windows. Because these systems are extremely complex (i.e. RFB performance is not only a function of the stability of the redox species, but also the supporting electrolyte, solvent, cell design, and so forth), it will be necessary to include methods for high-throughput synthesis, optimization and characterizations to gain these necessary fundamental insights through careful control of each of the components.

Regarding the development of ORMs, the choice of available materials and the complexity of the solvent environment highlight the need for developing highly efficient methods in material preparation, molecular screening, and system optimization. High-throughput synthesis and characterizations have yet not been explored. On the other hand, screening of electronic and steric parameters of a ORM family through machine learning and computational modeling allows for the prediction of high-performing molecules without an exhaustive search or dependence on fortuity. This strategy has been shown by the Sigman group on various occasions.<sup>65,99,102</sup> Notably, through the development of models

using quantitative structure-property relationships, they were able to predict both highly stable cycling pyridinium derivatives (no apparent degradation through 200 cycles when compared to 35% decomposition of the parent compound) as well as highly soluble cyclopropenium species (importantly shown across multiple charge states with >1.6 M monomer and >1.1 M dimer in both states). These studies show the utility of computational modelling for understanding and modulating the parameters, which affect multiple variables accounting for the energy and power density of NAqORFBs. Future application of these techniques is a powerful tool for ROM development and will be important for the isolation of ORMs with potential for commercial application.

In addition to the necessity of developing high-throughput tools for the preparation of versatile ORMs, the system cost is another parameter to be considered for widespread implementation. For instance, although ORMs are made of earth-abundant elements and therefore are potentially cheap, the cost of high purity of solvent and supporting electrolytes can be nontrivial. Moreover, since the operating environment has high requirements in oxygen and water level, the utilization of associated equipment together with the maintenance may also greatly increase the expense of the whole battery system. In summary, recent advancements have demonstrated the great potential of NAqORFBs in energy storage, yet there remain important opportunities for growth.

### Conclusions

To date, extensive advances have been made in NAqORFBs that have positioned this battery system as a promising solution in energy storage. To address issues encountered in these NAqORFBs, recent efforts have been focused to (1) improve solubility to prepare low melting-point or even liquid materials (e.g., eutectic mixtures), (2) extend redox potential differences for large cell voltage output (e.g., utilization of substituent effects on tuning redox potential, and exploration of new catholytes such as cyclopropenium), (3) access to second electron transfers for high energy storage (e.g., conjugation and adding EDGs), (4) mitigate active-molecule crossover (e.g., macromolecular design, bipolar redoxmers), and (5) enhance stability for long service lifetime (e.g., charge delocalization and steric protection). These advancements have resulted in ORMs with superior electrochemical properties such as large potential window ( $\geq 3V$ ) and high solubility ( $\geq 1.0 M$ ). Accordingly, NAqORFBs have opened an avenue in achieving high energy density. Compared to commercial VRFBs that exhibit energy density of 35 Wh L<sup>-1</sup>,<sup>35</sup> the energy density of NAqORFBs has been reported up to 200 Wh L<sup>-1</sup>,<sup>103, 104</sup>

However, to further reduce barriers impeding the use of NAqORFBs for practical applications, a number of challenges remain to be resolved. For example, although non-aqueous system allows for large battery voltage, the power density demonstrated to date (1 -10 m W cm<sup>-2</sup>) is not competitive with vanadium RFBs (up to 600 m W cm<sup>-2</sup>).<sup>21,105</sup> This is mainly due to

the low solution conductivity (40 – 55 mS/cm) and low membrane conductivity (0.1 – 20 mS/cm) in non-aqueous systems. Organic molecules offer great opportunities in structural functionalization, yet synthesis and molecular screening of a large variety of candidates are often tedious and time-consuming. Further complicating the study is molecular decomposition, which often has a detrimental effect on cycling lifetime. Additionally, although organic redox-active materials can be potentially cost-effective, cost evaluation for potential implementation is rare. Given the relevance of material characterization to understand reaction dynamics, integration of in-situ molecular screening that permits such observation at different time points would be of major interest to the field. Furthermore, the development of techniques to enable synthesis and characterization operated in a high-throughput mode will facilitate system optimization. Finally, although computational modeling has been reported to unravel experimental observation, advancement in developing models for property prediction would be of importance. In summary, recent advancements in NAQORFBs has promised great potential in energy storage, yet much is still to be done for widespread applications.

### Conflicts of interest

There are no conflicts to declare.

### Acknowledgements

The authors would like to thank for the Joint Center for Energy Storage Research (JCESR), which is funded by the U.S. Department of Energy, Office of Science, Basic Energy Sciences.

### References

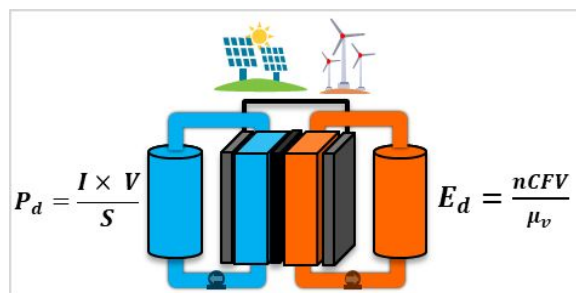
- J. A. Luo, B. Hu, M. W. Hu, Y. Zhao and T. L. Liu, *Acs Energy Lett*, 2019, **4**, 2220-2240.
- R. Chen, *Curr Opin Electrochem*, 2020, **21**, 40-45.
- D. G. Kwabi, Y. Ji and M. J. Aziz, *Chem Rev*, 2020, DOI: 10.1021/acs.chemrev.9b00599.
- P. Liu, Y. L. Cao, G. R. Li, X. P. Gao, X. P. Ai and H. X. Yang, *ChemSusChem*, 2013, **6**, 802-806.
- W. Wang, Q. T. Luo, B. Li, X. L. Wei, L. Y. Li and Z. G. Yang, *Adv Funct Mater*, 2013, **23**, 970-986.
- Y. Ding, C. K. Zhang, L. Y. Zhang, Y. G. Zhou and G. H. Yu, *Chem*, 2019, **5**, 1964-1987.
- J. Y. Ye, L. Xia, C. Wu, M. Ding, C. K. Jia and Q. Wang, *J Phys D Appl Phys*, 2019, **52**, 443001.
- C. K. Zhang, L. Y. Zhang, Y. Ding, S. S. Peng, X. L. Guo, Y. Zhao, G. H. He and G. H. Yu, *Energy Storage Mater*, 2018, **15**, 324-350.
- G. L. Soloveichik, *Chem Rev*, 2015, **115**, 11533-11558.
- Q. Zhao, Z. Zhu and J. Chen, *Adv Mater*, 2017, **29**, 1607007.
- R. Yan and Q. Wang, *Adv Mater*, 2018, **30**, e1802406.
- X. L. Wei, W. X. Pan, W. T. Duan, A. Hollas, Z. Yang, B. Li, Z. M. Nie, J. Liu, D. Reed, W. Wang and V. Sprenkle, *Acs Energy Lett*, 2017, **2**, 2187-2204.
- K. Lourensen, J. Williams, F. Ahmadpour, R. Clemmer and S. Tasnim, *J Energy Storage*, 2019, **25**, 100844.
- C. Minke and T. Turek, *J Power Sources*, 2018, **376**, 66-81.
- M. Ulaganathan, V. Aravindan, Q. Y. Yan, S. Madhavi, M. Skyllas-Kazacos and T. M. Lim, *Adv Mater Interfaces*, 2016, **3**, 1500309.
- P. Leung, A. A. Shah, L. Sanz, C. Flox, J. R. Morante, Q. Xu, M. R. Mohamed, C. P. de Leon and F. C. Walsh, *J Power Sources*, 2017, **360**, 243-283.
- R. F. Service, *Science*, 2014, **344**, 352-354.
- J. Winsberg, T. Hagemann, T. Janoschka, M. D. Hager and U. S. Schubert, *Angew Chem Int Ed*, 2017, **56**, 686-711.
- B. Huskinson, M. P. Marshak, C. Suh, S. Er, M. R. Gerhardt, C. J. Galvin, X. Chen, A. Aspuru-Guzik, R. G. Gordon and M. J. Aziz, *Nature*, 2014, **505**, 195-198.
- M. Park, J. Ryu, W. Wang and J. Cho, *Nat Rev Mater*, 2016, **2**, 1-18.
- Y. Ding, C. Zhang, L. Zhang, Y. Zhou and G. Yu, *Chem Soc Rev*, 2018, **47**, 69-103.
- H. Peng, Q. Yu, S. Wang, J. Kim, A. E. Rowan, A. K. Nanjundan, Y. Yamauchi and J. Yu, *Adv Sci* 2019, **6**, 1900431.
- B. Hu, C. DeBruler, Z. Rhodes and T. L. Liu, *J Am Chem Soc*, 2017, **139**, 1207-1214.
- C. DeBruler, B. Hu, J. Moss, X. Liu, J. Luo, Y. Sun and T. L. Liu, *Chem*, 2017, **3**, 961-978.
- X. Q. Xing, Q. H. Liu, B. G. Wang, J. P. Lemmon and W. Q. Xu, *J Power Sources*, 2020, **445**, 227330.
- X. Wei, W. Xu, J. Huang, L. Zhang, E. Walter, C. Lawrence, M. Vijayakumar, W. A. Henderson, T. Liu, L. Cosimbescu, B. Li, V. Sprenkle and W. Wang, *Angew Chem Int Ed*, 2015, **54**, 8684-8687.
- J. S. Yuan, C. J. Zhang, Y. H. Zhen, Y. C. Zhao and Y. D. Li, *J Power Sources*, 2019, **443**, 227283.
- S. Gentil, D. Reynard and H. H. Girault, *Curr Opin Electrochem*, 2020, **21**, 7-13.
- S. R. Narayan, A. Nirmalchandar, A. Murali, B. Yang, L. Hooper-Burkhardt, S. Krishnamoorthy and G. K. S. Prakash, *Curr Opin Electrochem*, 2019, **18**, 72-80.
- V. Singh, S. Kim, J. Kang and H. R. Byon, *Nano Res*, 2019, **12**, 1988-2001.
- K. Gong, Q. R. Fang, S. Gu, S. F. Y. Li and Y. S. Yan, *Energy Environ Sci*, 2015, **8**, 3515-3530.
- J. A. Kowalski, L. Su, J. D. Milshtein and F. R. Brushett, *Curr Opin Chem Eng*, 2016, **13**, 45-52.
- Y. P. Wang, M. Frascioni and J. F. Stoddart, *Acs Central Sci*, 2017, **3**, 927-935.
- Y. Y. Lai, X. Li and Y. Zhu, *Acs Appl Polym Mater*, 2020, **2**, 113-128.
- X. Wei, W. Xu, M. Vijayakumar, L. Cosimbescu, T. Liu, V. Sprenkle and W. Wang, *Adv Mater*, 2014, **26**, 7649-7653.
- W. T. Duan, J. H. Huang, J. A. Kowalski, I. A. Shkrob, M. Vijayakumar, E. Walter, B. F. Pan, Z. Yang, J. D. Milshtein, B. Li, C. Liao, Z. C. Zhang, W. Wang, J. Liu, J. S. Moore, F. R. Brushett, L. Zhang and X. L. Wei, *Acs Energy Lett*, 2017, **2**, 1156-1161.
- F. R. Brushett, J. T. Vaughey and A. N. Jansen, *Adv Energy Mater*, 2012, **2**, 1390-1396.
- L. Zhang, Z. C. Zhang, P. C. Redfern, L. A. Curtiss and K. Amine, *Energy Environ Sci*, 2012, **5**, 8204-8207.
- J. H. Huang, L. Su, J. A. Kowalski, J. L. Barton, M. Ferrandon, A. K. Burrell, F. R. Brushett and L. Zhang, *J Mater Chem A*, 2015, **3**, 14971-14976.
- J. H. Huang, L. Cheng, R. S. Assary, P. Q. Wang, Z. Xue, A. K. Burrell, L. A. Curtiss and L. Zhang, *Adv Energy Mater*, 2015, **5**, 1401782.
- J. D. Milshtein, A. P. Kaur, M. D. Casselman, J. A. Kowalski, S. Modekrutti, P. L. Zhang, N. H. Attanayake, C. F. Elliott, S. R. Parkin, C. Risko, F. R. Brushett and S. A. Odom, *Energy Environ Sci*, 2016, **9**, 3531-3543.

- 42 P. Geysens, Y. Li, I. Vankelecom, J. Fransaer and K. Binnemans, *ACS Sus Chem Eng*, 2020, **8**, 3832-3843.
- 43 X. L. Wei, W. T. Duan, J. H. Huang, L. Zhang, B. Li, D. Reed, W. Xu, V. Sprenkle and W. Wang, *Acs Energy Lett*, 2016, **1**, 705-711.
- 44 C. K. Zhang, Z. H. Niu, Y. Ding, L. Y. Zhang, Y. G. Zhou, X. L. Guo, X. H. Zhang, Y. Zhao and G. H. Yu, *Chem*, 2018, **4**, 2814-2825.
- 45 C. Zhang, Y. Qian, Y. Ding, L. Zhang, X. Guo, Y. Zhao and G. Yu, *Angew Chem Int Ed*, 2019, **58**, 7045-7050.
- 46 N. H. Attanayake, J. A. Kowalski, K. V. Greco, M. D. Casselman, J. D. Milshtein, S. J. Chapman, S. R. Parkin, F. R. Brushett and S. A. Odom, *Chem Mater*, 2019, **31**, 4353-4363.
- 47 G. Kwon, K. Lee, M. H. Lee, B. Lee, S. Lee, S. K. Jung, K. Ku, J. Kim, S. Y. Park, J. E. Kwon and K. Kang, *Chem*, 2019, **5**, 2642-2656.
- 48 A. Shimizu, K. Takenaka, N. Handa, T. Nokami, T. Itoh and J. I. Yoshida, *Adv Mater*, 2017, **29**, 1606592.
- 49 A. Abo-Hamad, M. Hayyan, M. A. AlSaadi and M. A. Hashim, *Chem Eng J*, 2015, **273**, 551-567.
- 50 C. K. Zhang, L. Y. Zhang, Y. Ding, X. L. Guo and G. H. Yu, *Acs Energy Lett*, 2018, **3**, 2875-2883.
- 51 R. M. Darling, K. G. Gallagher, J. A. Kowalski, S. Ha and F. R. Brushett, *Energ Environ Sci*, 2014, **7**, 3459-3477.
- 52 J. L. Zhang, R. E. Corman, J. K. Schuh, R. H. Ewoldt, I. A. Shkrob and L. Zhang, *J Phys Chem C*, 2018, **122**, 8159-8172.
- 53 G. Nagarjuna, J. Hui, K. J. Cheng, T. Lichtenstein, M. Shen, J. S. Moore and J. Rodriguez-Lopez, *J Am Chem Soc*, 2014, **136**, 16309-16316.
- 54 W. T. Duan, R. S. Vemuri, J. D. Milshtein, S. Laramie, R. D. Dmello, J. H. Huang, L. Zhang, D. H. Hu, M. Vijayakumar, W. Wang, J. Liu, R. M. Darling, L. Thompson, K. Smith, J. S. Moore, F. R. Brushett and X. L. Wei, *J Mater Chem A*, 2016, **4**, 5448-5456.
- 55 K. H. Hendriks, C. S. Sevov, M. E. Cook and M. S. Sanford, *Acs Energy Lett*, 2017, **2**, 2430-2435.
- 56 C. Hansch, A. Leo and R. W. Taft, *Chem Rev*, 1991, **91**, 165-195.
- 57 D. Job and H. B. Dunford, *Eur J Biochem*, 1976, **66**, 607-614.
- 58 S. M. Batterjee, M. I. Marzouk, M. E. Aazab and M. A. El-Hashash, *Appl Organomet Chem*, 2003, **17**, 291-297.
- 59 R. Lincoln, L. E. Greene, K. Krumova, Z. Ding and G. Cosa, *J Phys Chem A*, 2014, **118**, 10622-10630.
- 60 J. Huang, A. N. L. Cheng, I. A. Shkrob, X. Xue, J. Zhang, N. R. Dietz Rago, L. A. Curtiss, K. Amine, Z. Zhang and L. Zhang, *J Mater Chem A*, 2015, **3**, 10710-10714.
- 61 M. D. Casselman, A. P. Kaur, K. A. Narayana, C. F. Elliott, C. Risko and S. A. Odom, *Phys Chem Chem Phys*, 2015, **17**, 6905-6912.
- 62 M. D. Casselman, C. F. Elliott, S. Modekrutti, P. L. Zhang, S. R. Parkin, C. Risko and S. A. Odom, *Chemphyschem*, 2017, **18**, 2142-2146.
- 63 J. Huang, Z. Yang, M. Vijayakumar, W. Duan, A. Hollas, B. Pan, W. Wang, X. Wei and L. Zhang, *Adv Sustain Syst*, 2018, **2**, 1700131.
- 64 C. S. Sevov, S. K. Samaroo and M. S. Sanford, *Adv Energy Mater*, 2017, **7**, 1602027.
- 65 Y. Yan, S. G. Robinson, M. S. Sigman and M. S. Sanford, *J Am Chem Soc*, 2019, **141**, 15301-15306.
- 66 J. Winsberg, S. Benndorf, A. Wild, M. D. Hager and U. S. Schubert, *Macromol Chem Phys*, 2018, **219**, 1700267.
- 67 J. A. Kowalski, M. D. Casselman, A. P. Kaur, J. D. Milshtein, C. F. Elliott, S. Modekrutti, N. H. Attanayake, N. J. Zhang, S. R. Parkin, C. Risko, F. R. Brushett and S. A. Odom, *J Mater Chem A*, 2017, **5**, 24371-24379.
- 68 R. A. Potash, J. R. McKone, S. Conte and H. D. Abruna, *J Electrochem Soc*, 2016, **163**, A338-A344.
- 69 C. G. Armstrong and K. E. Toghiani, *J Power Sources*, 2017, **349**, 121-129.
- 70 J. A. Suttill, J. F. Kucharyson, I. L. Escalante-Garcia, P. J. Cabrera, B. R. James, R. F. Savinell, M. S. Sanford and L. T. Thompson, *J Mater Chem A*, 2015, **3**, 7929-7938.
- 71 J. Kucharyson, Structure-Function Relationships of Metal Coordination Complexes for Non-Aqueous Redox Flow Batteries. University of Michigan, 2017, 272 P. <http://hdl.handle.net/2027.42/137020>.
- 72 R. W. Hogue and K. E. Toghiani, *Curr Opin Electrochem*, 2019, **18**, 37-45.
- 73 J. Huang, B. Pan, W. Duan, X. Wei, R. S. Assary, L. Su, F. R. Brushett, L. Cheng, C. Liao, M. S. Ferrandon, W. Wang, Z. Zhang, A. K. Burrell, L. A. Curtiss, I. A. Shkrob, J. S. Moore and L. Zhang, *Sci Rep*, 2016, **6**, 32102.
- 74 K. Hernández-Burgos, G. G. Rodríguez-Calero, W. Zhou, S. E. Burkhardt and H. D. Abruña, *J Am Chem Soc*, 2013, **135**, 14532-14535.
- 75 T. Sukegawa, I. Masuko, K. Oyaizu and H. Nishide, *Macromolecules*, 2014, **47**, 8611-8617.
- 76 J. Winsberg, T. Hagemann, S. Muench, C. Friebe, B. Haupler, T. Janoschka, S. Morgenstern, M. D. Hager and U. S. Schubert, *Chem Mater*, 2016, **28**, 3401-3405.
- 77 E. C. Montoto, Y. Cao, K. Hernandez-Burgos, C. S. Sevov, M. N. Braten, B. A. Helms, J. S. Moore and J. Rodriguez-Lopez, *Macromolecules*, 2018, **51**, 3539-3546.
- 78 M. Burgess, E. Chenard, K. Hernandez-Burgos, G. Nagarjuna, R. S. Assary, J. S. Hui, J. S. Moore and J. Rodriguez-Lopez, *Chem Mater*, 2016, **28**, 7362-7374.
- 79 E. C. Montoto, G. Nagarjuna, J. S. Moore and J. Rodriguez-Lopez, *J Electrochem Soc*, 2017, **164**, A1688-A1694.
- 80 M. Burgess, J. S. Moore and J. Rodriguez-Lopez, *Accounts Chem Res*, 2016, **49**, 2649-2657.
- 81 M. J. Baran, M. N. Braten, E. C. Montoto, Z. T. Gossage, L. Ma, E. Chenard, J. S. Moore, J. Rodriguez-Lopez and B. A. Helms, *Chem Mater*, 2018, **30**, 3861-3866.
- 82 S. E. Doris, A. L. Ward, A. Baskin, P. D. Frischmann, N. Gavvalapalli, E. Chenard, C. S. Sevov, D. Prendergast, J. S. Moore and B. A. Helms, *Angew Chem Int Ed*, 2017, **56**, 1595-1599.
- 83 K. H. Hendriks, S. G. Robinson, M. N. Braten, C. S. Sevov, B. A. Helms, M. S. Sigman, S. D. Minter and M. S. Sanford, *ACS Cent Sci*, 2018, **4**, 189-196.
- 84 E. C. Montoto, G. Nagarjuna, J. S. Hui, M. Burgess, N. M. Sekerak, K. Hernandez-Burgos, T. S. Wei, M. Kneer, J. Grolman, K. J. Cheng, J. A. Lewis, J. S. Moore and J. Rodriguez-Lopez, *J Am Chem Soc*, 2016, **138**, 13230-13237.
- 85 Z. T. Gossage, K. Hernandez-Burgos, J. S. Moore and J. Rodriguez-Lopez, *Chemelectrochem*, 2018, **5**, 3006-3013.
- 86 P. Navalpotro, J. Palma, M. Anderson and R. Marcilla, *Angew Chem Int Ed*, 2017, **56**, 12460-12465.
- 87 P. Navalpotro, N. Sierra, C. Trujillo, I. Montes, J. Palma and R. Marcilla, *Acs Appl Mater Inter*, 2018, **10**, 41246-41256.
- 88 S. H. Oh, C. W. Lee, D. H. Chun, J. D. Jeon, J. Shim, K. H. Shin and J. H. Yang, *J Mater Chem A*, 2014, **2**, 19994-19998.
- 89 J. Winsberg, C. Stolze, S. Muench, F. Liedl, M. D. Hager and U. S. Schubert, *Acs Energy Lett*, 2016, **1**, 976-980.
- 90 S. Hwang, H. S. Kim, J. H. Ryu and S. M. Oh, *J Power Sources*, 2018, **395**, 60-65.
- 91 G. D. Charlton, S. M. Barbon, J. B. Gilroy and C. A. Dyker, *J Energy Chem*, 2019, **34**, 52-56.
- 92 Y. Z. Zhu, F. Yang, Z. H. Niu, H. X. Wu, Y. He, H. F. Zhu, J. Ye, Y. Zhao and X. H. Zhang, *J Power Sources*, 2019, **417**, 83-89.
- 93 C. G. Armstrong and K. E. Toghiani, *Journal*, 2018, **91**, 19-24.

## ARTICLE

## Journal Name

- 94 C. G. Armstrong and K. E. Toghill, *Electrochem Commun*, 2018, **91**, 19-24.
- 95 G. Kwon, S. Lee, J. Hwang, H. S. Shim, B. Lee, M. H. Lee, Y. Ko, S. K. Jung, K. Ku, J. Hong and K. Kang, *Joule*, 2018, **2**, 1771-1782.
- 96 Z. Li, S. Li, S. Q. Liu, K. L. Huang, D. Fang, F. C. Wang and S. Peng, *Electrochem Solid St*, 2011, **14**, A171-A173.
- 97 K. A. Narayana, M. D. Casselman, C. F. Elliott, S. Ergun, S. R. Parkin, C. Risko and S. A. Odom, *Chemphyschem*, 2015, **16**, 1179-1189.
- 98 C. S. Sevov, R. E. Brooner, E. Chenard, R. S. Assary, J. S. Moore, J. Rodriguez-Lopez and M. S. Sanford, *J Am Chem Soc*, 2015, **137**, 14465-14472.
- 99 C. S. Sevov, D. P. Hickey, M. E. Cook, S. G. Robinson, S. Barnett, S. D. Minter, M. S. Sigman and M. S. Sanford, *J Am Chem Soc*, 2017, **139**, 2924-2927.
- 100 C. S. Sevov, S. K. Samaroo and M. S. Sanford, *Advanced Energy Materials*, 2017, **7**, 1602027.
- 101 Y. Yan, S. G. Robinson, M. S. Sigman and M. S. Sanford, *J Am Chem Soc*, 2019, **141**, 15301-15306.
- 102 S. G. Robinson and M. S. Sigman, *Acc Chem Res*, 2020, **53**, 289-299.
- 103 X. Q. Xing, Q. H. Liu, W. Q. Xu, W. B. Liang, J. Q. Liu, B. G. Wang and J. P. Lemmon, *Acs Appl Energ Mater*, 2019, **2**, 2364-2369.
- 104 K. Takechi, Y. Kato and Y. Hase, *Adv Mater*, 2015, **27**, 2501-2506.
- 105 H. R. Jiang, J. Sun, L. Wei, M. C. Wu, W. Shyy and T. S. Zhao, *Energy Storage Mater*, 2020, **24**, 529-540.



The state-of-art advances of non-aqueous organic redox flow batteries for grid-scale energy storage were evaluated and summarized.